NanoMi: an open source electron microscope hardware and software platform

Malac, Marek; Calzada, Jesus Alejandro Marin; Salomons, Mark; Homeniuk, Darren; Price, Patrick; Cloutier, Martin; Hayashida, Misa; Vick, Doug; Chen, Sean; Yakubu, Suliat; Wen, Zhengxu (Darren); Leeson, Marcus; Kamal, Mohammad; Pitters, Jason; Kim, John; Wang, Xuanhao; Adkin-Kaya, Olivier; Egerton, Ray

Publisher's version / Version de l'éditeur:
https://doi.org/10.1016/j.micron.2022.103362
Micron, 163, C, pp. 1-25, 2022-10-04

NanoMi: An Open Source Electron Microscope Hardware and Software Platform.

Marek Malac

NRC-NANO, National Research Council, Edmonton, Alberta, T6G 2M9, Canada

Department of Physics, University of Alberta, Edmonton, Alberta, T6G 2E1, Canada

Jesus Alejandro Marin Calzada

Department of Physics, University of Alberta, Edmonton, Alberta, T6G 2E1, Canada

Mark Salomons

NRC-NANO, National Research Council, Edmonton, Alberta, T6G 2M9, Canada

Darren Homeniuk

NRC-NANO, National Research Council, Edmonton, Alberta, T6G 2M9, Canada

Patrick Price

NRC-NANO, National Research Council, Edmonton, Alberta, T6G 2M9, Canada

Martin Cloutier

NRC-NANO, National Research Council, Edmonton, Alberta, T6G 2M9, Canada

Misa Hayashida

NRC-NANO, National Research Council, Edmonton, Alberta, T6G 2M9, Canada

Doug Vick

Email addresses: marek.malac@nrc-cnrc.gc.ca / mmalac@ualberta.ca (Marek Malac), marincal@ualberta.ca (Jesus Alejandro Marin Calzada), Mark.Salomons@nrc-cnrc.gc.ca (Mark Salomons), Darren.Homeniuk@nrc-cnrc.gc.ca (Darren Homeniuk), Patrick.Price@nrc-cnrc.gc.ca (Patrick Price), martin.cloutier@nrc-cnrc.gc.ca (Martin Cloutier), Misa.Hayashida@nrc-cnrc.gc.ca (Misa Hayashida), Douglas.Vick@nrc-cnrc.gc.ca (Doug Vick), seanyuehshengchen3@gmail.com (Sean Chen), suliat.f.yakubu@gmail.com (Suliat Yakubu), darrenwen2013@gmail.com (Zhengxu (Darren) Wen), leesonmarcus@gmail.com (Marcus Leeson), mkamal@ualberta.ca (Mohammad Kamal), johnkm37@gmail.com (John Kim), regerton@ualberta.ca (Ray Egerton)

NRC-NANO, National Research Council, Edmonton, Alberta, T6G 2M9, Canada

Sean Chen

UBC Department of Physics & Astronomy 6224 Agricultural Road, Vancouver BC, V6T 1Z1, Canada

Suliat Yakubu

School of Biomedical Engineering The University of British Columbia 2335 Engineering Rd X015 Vancouver BC, V6T 1Z4 Canada

Zhengxu (Darren) Wen

Integrated Engineering Program, The University of British Columbia, 6350 Stores Road, Vancouver, BC, V6T 2B4, Canada

Marcus Leeson

Faculty of Mechanical Engineering University of British Columbia, 6250 Applied Science Lane, Vancouver, Canada

Mohammad Kamal

Department of Electrical and Computer Engineering, University of Alberta, 9211 116 Street NW Edmonton, T6G 1H9, Canada

John Kim

Department of Electrical and Computer Engineering, The University of British Columbia, 5500 – 2332 Main Mall Vancouver, BC V6T 1Z4, Canada

Ray Egerton

Department of Physics, University of Alberta, Edmonton, Alberta, T6G 2E1, Canada

---

Abstract

We outline a public license (open source) electron microscopy platform, referred to as NanoMi. NanoMi offers a modular, flexible electron microscope platform that can be utilized for a variety of applications, such as microscopy education and development of proof-of-principle experiments, and can be used to complement an existing experimental apparatus. All components are ultra-high vacuum compatible and the electron optics elements are independent from the vacuum envelope. The individual optical components are mounted on a 5-inch diameter half-pipe, allowing customizing of electron optics for a variety of purposes. The target capabilities include SEM, TEM, scanning TEM (STEM), and ED (ED) at up to 50 keV incident electron energy. The intended image resolution in SEM, TEM and STEM modes is ≈10 nm. We describe the existing components and the interfaces among components that ensure their compatibility and interchangeability. The paper provides a resource for those who consider building or utilizing their own NanoMi.

Keywords: Transmission electron microscope (TEM), Scanning Electron Microscope (SEM), Scanning Transmission Electron Microscope (STEM), ED, Public License Electron Microscope, Open Science, Microscopy Education.

---

1. Introduction

Electron microscopy (EM) offers imaging and analytical capabilities down to the atomic length scale Reimer (1998), Kohl and Reimer (2008), Carter and Williams (2016), Edington (1974, 1975a,b, 1976), Thompson-Russell and Edington (1977), Hall (1966), Hawkes and Valdre (1990). Its origins trace to the 1930s Hawkes and Kasper (1994), Grivet (1972), Valdre and Zichich (1971), Hawkes and Kasper (1994), Rose (2009), Siegel (1964). Arguably, the field of EM would benefit from EM instrumentation that can be easily customized, and that exposes physical concepts underlying electron microscopy Egerton (2005). Modern high-end transmission electron microscopes (TEM) and scanning TEM (STEM) are typically housed in a multi user facility, sometimes with limited opportunities to extensively explore and customize the instrument. NanoMi aims to provide an instrument where EM concepts can be readily observed and hardware (HW) directly controlled by transparent and customizable software (SW), even when the main objective is the acquisition of application data. The low cost of NanoMi makes it accessible to students early in their curriculum, learning EM principles and developing skills needed to use a variety of instruments in their career.

Furthermore, there is a lack of customizable instrumentation that could provide EM imaging capabilities for ultra high vacuum (UHV) growth chambers, mass spectrometers, and various multi probe instruments, e.g. UHV and low temperature atomic force microscopes (AFM) and scanning tunneling microscopes (STM). Such instruments are often custom built or heavily modified, but there are limited means to add affordable and customizable SEM and TEM capability.

The progress, affordability and availability of UHV hardware, oil-free vacuum pumps, improved stability of solid state electronics and high voltage (HV) power supplies, and computer control HW and SW are key in enabling NanoMi. Ever increasing interest in open science and open license HW and SW further motivate the development of NanoMi.

NanoMi aims to contribute to development of EM and its applications by providing a public license, modest resolution, EM column that can be extensively modified, easily disassembled and reconfigured Open Science Foundation (0000), NanoMi (0000), Malac et al. (2020, 2021, 2022). The NanoMi components can perhaps facilitate development of public license ion beam column and electron beam lithography (EBL) tools. However, NanoMi is unlikely to become competitive with commercial instruments in terms of performance, convenience of use and service support. Throughout the manuscript we strive to provide references to open access literature, making use of the fact that many EM concepts can be found in well-aged books, that are posted for example at `archive.org`. It should be noted that while all components discussed here are completed, the entire instrument integration is still a work in progress.

2. NanoMi Design Considerations, Layout and Component Interfaces.

In this section, we discuss the consideration underlying NanoMi design, the reasons for using electrostatic (ES) optics and the electrical stability, mechanical tolerances and aberrations budget for target performance. We also describe the interfaces between NanoMi subsystems.

Fig. 1 shows a photo of the first NanoMi column. It is based on 6-inch (6”) diameter ConFlat (CF) tubing with 8” diameter CF flanges. All components except for the bottom section, where the electron source is located, are standard *off-the-shelf* CF components. The column in Fig. 1a) is sufficient to accommodate scanning electron microscope (SEM), TEM, STEM and electron diffraction (ED) capabilities. It is ≈1300 mm tall. The probe forming section of the column, as needed for SEM alone, is ≈500 mm tall, but individual configurations can vary in size. For example, if the maximum acceleration potential U_0 is decreased from the target 50 kV, the column size can be reduced. Fig. 1b) shows Einzel lens and a sample stage attached to a 5" diameter half-pipe breadboard that supports all electron-optical and mechanical components, and is suspended inside the 6" diameter CF tubing.

Simplicity, ease of manufacturing, assembly and alignment, clarity of microscopy concepts and safety considerations guided NanoMi design choices and approaches.

2.1. Choice of Electron Optics

Here we briefly discuss the reasons for choosing electrostatic, rather than magnetic lenses for the first NanoMi[1]. Both electric and magnetic fields can be used to deflect and focus electron beams Rose (2009), Egerton (2011, 2005), Liebl (2007), Hawkes and Kasper (1994), Delong and Lencova (2021), Baranova and Yavor (1989), Grivet (1972), ed. (2009), Valdre and Zichich (1971), Septier (1967). Table 2.1 summarizes the advantages and drawbacks of electrostatic, magnetic coil-excited and permanent magnet-excited magnetic lenses. For a low-voltage ($U_0 \leq 50$ kV) microscope with modest resolution where easy build process is a critical requirement, electrostatic Einzel lenses appear to provide a suitable solution Liebl (2007), Rempfer (1985), Hawkes and Kasper (1994), Rose (2009), Baranova and Yavor (1989). Similarly, deflectors and stigmators utilizing electric fields are not complicated to implement.

2.2. Effect of Aberrations and Disturbances on SEM and STEM Probe Size

Here we discuss the requirements on lens aberrations and high voltage (HV) power supply stability required to achieve the target ≈10 nm probe diameter in SEM and STEM and ≈10 nm resolution in TEM. Manufacturing and alignment precision are considered in Section 4.

Forming a small probe in SEM and STEM requires the electron source to be sufficiently demagnified and focused into a small spot at the sample plane. Source demagnificaiton is discussed in Section 3.1. Ultimately, the smallest size of the probe at sample plane is limited by diffraction of the electron beam at apertures and by aberrations of the probe-forming lens Reimer (1998), Kohl and Reimer (2008), Egerton (2005), Kirkland (2020),

[1]Magnetic deflectors, stigmators and lenses, including ones excited by a permanent magnet, can be utilized in future versions of NanoMi.

	Electrostatic	**Magnetic, coil excitation**	**Magnetic, permanent magnet excitation**
Manufacturing	Three concentric apertures are sufficient. Electrical insulation is required.	Complicated magnetic circuit is required. Magnetic circuit must be accurately positioned within a coil with hundreds to thousands turn winding.	Complicated magnetic circuit is required. Precise positioning of permanent magnet and magnetic circuit is required.
Lens material	Any conductor. Copper, aluminium or non magnetic stainless steel are suitable.	High quality permalloy.	High quality permalloy.
Lens excitation	High voltage up to U_0.	Low voltage, magnetic coil, current a few Amperes.	Permanent magnet.
Driving circuit	Individual high voltage supply for each lens, or divider utilizing single U_0 power supply for all lens.[2]	Low voltage direct current current power supply.	Not applicable.
Focusing	By varying lens voltage.	By varying lens current.	By mechanical positioning.
Force	$q\vec{E}$, Suitable also for ion optics.	$q\vec{v} \times \vec{B}$	$q\vec{v} \times \vec{B}$
Cooling	Not needed	Water cooling for high-excitation, short focal length lens.	Not needed.
Charging instabilities	Serious issue if using oil-sealed pumps, or when vacuum is poor. Increases with increasing U_0. Usually not problematic below 30 kV and manageable to perhaps 100 kV.	Not a major issue, lens bore is a conductor at ground potential.	Not a major issue, lens bore is a conductor at ground potential.
Time constant for lens, deflectors and stigmators	Low ($\leq$ μs) for deflectors and stigmators, ms for strong lens.	High (ms for stigmators and deflectors, tens to hundreds of ms for a strong lens.)	∞
Advantages	Extensive knowledge available from days of CRTs television sets, and from early electron microscopes. Many patents are expired.	Suitable for high performance microscopes. Suitable for microscopes operated up to 3 MeV.	Strong lens without cooling maybe possible.
Limitations	Not suitable for operation above ≈100 kV.	Large coil needed to achieve short focal length. Can not be placed inside a vacuum chamber easily.	Can not focus easily.
Aberrations and focal length (f)	A few mm f is achievable in a simple Einzel lens	Sub-1mm f is possible in uncorrected (immersion) lens	Short focal may be length possible.
Immersion lens[3]	Not possible. Electric field of lens would be affected by sample shape and electrical properties.	Routinely used in high performance instruments. Can not be used for magnetic samples.	Maybe possible.
Typical minimum f, C_S and C_C parameters[4]	f_{min} ≈5 mm, C_S ≈10 to 50 mm, C_C ≈10 to 50 mm Rempfer (1985)	f_{min} ≈0.5 mm, C_S ≈1 mm, C_C ≈1 mm	Likely comparable to coil-excited magnetic lens, as determined by the magnetic circuit and magnetic properties of the permanent magnet.
Operation mode	Accelerating and decelerating mode Grivet (1972), Liebl (2007)	Always converging lens.	Always converging lens.

Table 1: Summary of advantages and drawbacks of electrostatic, magnetic coil-excited and permanent magnet-excited magnetic lens. Here f denotes lens focal length, C_S and C_C refer to spherical and chromatic aberration of a lens respectively.

Egerton and Watanabe (2022). For ≈10 nm probe size in NanoMi, primarily spherical aberration C_S and chromatic aberration C_C need to be considered Kirkland (2020). Spherical aberration refers to the fact that electrons travelling far from the optical axis are focused more strongly than those travelling close to the optical axis of the lens Egerton (2005), Reimer (1998), Kohl and Reimer (2008), Kirkland (2020), Fig. 2d) and e). As a result, a point source is imaged into a disc with finite size. Chromatic aberration refers to the fact that lens focal length depends on the wavelength and therefore energy of the electrons that are focused. Consequently, an electron source with a finite width energy distribution, $\Delta E \approx$2eV for W-hairpin filament Kohl and Reimer (2008), produces a blurred disc at the sample plane. To estimate the effect of C_S and C_C, we follow the approach outlined in Kirkland (2020), Chapter 3.

Using the applicable values of the C_S of an Einzel lens, see Rempfer (1985), we can estimate the smallest probe diameter for SEM and STEM. *Small* probe diameter can be defined, for example, as a diameter ($d_{Scherzer}$) under Scherzer conditions Kirkland (2020), that produces a small full width half maximum (FWHM) probe diameter while keeping the probe tails limited, see Fig. 3a) and Kirkland (2020), Egerton and Watanabe (2022). Alternatively, probe diameter can be defined as the smallest diameter containing 50% of the incident beam current Kirkland (2020), as used here[5].

Probe intensity $I(r)$ as a function of radial distance r from the centre of the probe can be obtained as Kirkland (2020):

$$I(r) = \int_0^{k_{max}} e^{-i\chi(k)} J_0(2\pi k r) k dk \tag{1}$$

E:ProbeInt

Here $k = \frac{1}{\lambda}$ is the electron wave vector, λ is the electron wavelength, J_0 is a Bessel function of the first kind. The aberration function $\chi(k)$ that includes only defocus Δz and spherical aberration C_S and was taken using the convention in Kirkland (2020) as:

$$\chi(k) = \pi \lambda k^2 \Big(\frac{C_S \lambda^2 k^2}{2} - \Delta z \Big) \tag{2}$$

E:Abber

The convention of Kirkland (2020), as used here, assigns a positive Δz underfocused (weaker than focused) lens. Spatial frequency k_{max} refers to

[5]It is possible to form a probe with extremely small FWHM at the expense of increasing intensity within the probe tails.

the maximum scattering vector allowed by the angle limiting aperture with a *semiangle* β with $\beta = \lambda k_{max}$ connecting the aperture semiangle and k_{max}. The Scherzer probe diameter $d_{Scherzer}$ and the conditions yielding it are Kirkland (2020):

$$d_{Scherzer} = 0.64(C_S\lambda^3)^{1/4} \tag{3}$$

obtained at Scherzer conditions:

$$\Delta z = 1.2\sqrt{C_S\lambda}$$

$$k_{max} = 1.56(C_S\lambda^3)^{-0.25}$$

E:Scherzer

The probe current $I_i(r)$ accounting for the increase in probe current with increasing radial distance r from the probe centre can be written as:

$$I_i(r) \approx 2\pi \int_0^\infty I(r')r'dr' \tag{4}$$

E:ProbeIntCurr

Eq. 4 can be used to estimate probe diameter d_{50} that contains 50% of the beam current and the conditions that yield the smallest d_{50}, see Kirkland (2020):

$$d_{50} = 0.86(C_S\lambda^3)^{1/4} \tag{5}$$

obtained at conditions yielding the smallest d_{50}:

$$\Delta z = 0.87\sqrt{C_S\lambda}$$

$$k_{max} = 1.34(C_S\lambda^3)^{-0.25}$$

E:d50

Probes with minimum $d_{Scherzer}$ or d_{50} optimize the probe broadening due to spherical aberration, that increases with beam convergence semiangle β, and diffraction broadening that increases with decrease in β Kirkland (2020), Egerton (2005), Kohl and Reimer (2008), Reimer (1998). Since NanoMi is intended for modest resolution imaging, the current distribution within the probe and consequently the d_{50} is a relevant measure of the practical probe diameter than $d_{Scherzer}$.

Fig. 3b) to e) shows a map of d_{50} for a lens with $C_S = 50$ mm for acceleration potential U_0 1 kV, 10 kV, 30 kV and 50 kV. The minimum achievable probe diameter decreases with increasing U_0 from $d_{50} \approx 4$ nm at $U_0 = 1$ kV down to $d_{50} \approx 1$ nm at U_0 50 kV. The d_{50} probe diameters are marked with contour lines with 1 nm increments in d_{50}. The maps in Fig. 3 indicate a patch of operating conditions that yield small d_{50} over the entire studied range of U_0 from 1 kV to 50 kV, indicated in dark gray in Fig. 3.

A practical NanoMi implementation may have only a few condenser aperture diameters installed at a given time. Typically the aperture opening diameter is between ≈ 10 μm and several hundred μm. For a given aperture diameter in μm the corresponding β

$$\beta = \frac{aperture\ diameter}{2(focal\ length)} \tag{6}$$

E:AngleAperture

Fig. 3 can be used to guide the choice of condenser aperture diameters that should be installed in NanoMi [6] to yield a small probe, see Fig. 3. As a numerical example, a 200 μm diameter aperture opening at the centre of a lens with $f = 10$ mm focal length[7] gives $\frac{200\mu m}{2\times 10mm} = 10$ mrad.

Fig. 3 further indicates that the smallest d_{50} is achieved at a positive defocus Δz between $\approx$10 nm and a few hundred nm. A large range of Δz that yields a small d_{50} at the sample indicates a large depth of focus for a given d_{50} Kohl and Reimer (2008). In practical terms, a large range of Δz that retains a small d_{50} amounts to convenient microscope operation. Fig. 3b) to e) indicate that the range of Δz allowing for small d_{50} increases with decreasing β. Fig. 3 b) to e) indicate that the C_S-limited d_{50} is smaller than the target $\approx$10 nm resolution even for a lens with a rather large $C_S \approx$50 mm. Even at $U_0 = 1$ kV, see Fig. 3b), a rather wide range of operating conditions, ($2\times\beta \approx$ 10 to 15 mrad and Δ_z from $\approx$200 nm to $\approx$1500 nm), yields $d_{50} \leq 4$ nm.

Having shown that aberrations (C_S and Δz) allow for sub-5 nm d_{50} we now turn attention to the effect of chromatic aberration C_C and high voltage instabilities on SEM and STEM probe size. We briefly discuss the requirements on stability of high voltage power supplies U_L controlling the Einzel lens focal length f and power supplies providing acceleration potential U_0.

[6] A decrease in condenser aperture diameter will also reduce the beam current and will result in increased noise in images.

[7] Alternatively an appropriately scaled aperture opening can be placed at a conjugated plane.

We discuss the noise requirements of scanning deflectors and their electronics as well as disturbances in probe positioning in Section 5.

A detailed investigation of Einzel lens C_C and the parameters which it depends on can be found in Rempfer (1985). For a simplified estimate below, we use $C_C = 28$ mm as applicable to NanoMi Einzel lenses in Section 3.3 and Figs. 2 and 7, operated at lens potential $U_L \approx 0.8 \times U_0$. An estimate of diameter d_C of SEM and STEM probe blurred due to chromatic aberration can be written as Kohl and Reimer (2008), Kirkland (2020):

$$d_C = \frac{1}{2}\beta C_C \sqrt{\left(\frac{\Delta E}{eU_0}\right)^2 + \left(\frac{\delta U_0}{U_0}\right)^2} \quad (7)$$

E:CcDisc

Here C_C is chromatic aberration coefficient of the lens, $2\times\beta$ is the angle of the electrons forming an image with the optical axis determined for example by the condenser aperture[8], δU_0 is the instability of the acceleration potential U_0, a value of $\frac{\delta U_0}{U_0} = 10$ ppm was used for the estimates in Fig. 3f). Additional terms for instabilities of various components can be added as needed Kohl and Reimer (2008). Fig. 3f) indicates that even for a rather high C_C, W-hairpin electron source and 10 ppm instabilities of U_0 a $d_C \leq 10$ nm can be achieved for realistic 2β over a wide range of U_0. In fact, the δU_0 has two main components, ripple of the HV power supply and its drift. Both components need to be within the δU_0 over the period of data acquisition. Nevertheless, HV power supplies meeting the parameters are accessible and affordable, see Section 14.

The effect of the term $\frac{\Delta E}{U_0}$ in Eq. 7 can be reduced for example by replacing the W-hairpin filament with a LaB_6 filament with $\Delta E \approx$1 eV, see table 4.1 in Kohl and Reimer (2008) [9].

In STEM the chromatic diameter d_C is primarily determined by the energy width of the electron source ΔE. Therefore, to decrease d_C the electron

[8] In STEM literature a condenser aperture is often referred to as an *objective aperture* reflecting the fact that it plays a role of an objective aperture in conventional TEM. Kirkland (2020)

[9] In our experience $\Delta E \approx$0.7 eV is achievable with an undersaturated LaB_6 filament. In some electron gun designs, a LaB_6 source is a drop-in replacement for a W-hairpin filament. Further improvement require use of Schottky or a cold field emission source, but they require significantly lower vacuum in the gun region thus increasing cost of the instrument.

source ΔE must be reduced. The reduction in ΔE can be achieved by either utilizing a field emission electron gun (FEG), or field-assisted thermal (Schottky) electron gun Kohl and Reimer (2008). Both FEG and Schottky guns require improved vacuum as provided by ion pumps, at least for the electron gun region of NanoMi. Alternatively a LaB_6 electron source combined with a monochromator could be considered Ogawa et al. (2022) at the expense of reduced beam current leading to increased pixel dwell time.

In STEM or SEM mode, energy broadening due to interactions within the sample has no effect on the achievable resolution. In TEM mode, energy broadening due to interaction of the electrons with the sample, and the resulting electron energy loss, has essentially the same effect as the increase of electron source energy width Egerton and Watanabe (2022), Hayashida and Malac (2022), Malac et al. (2021). Therefore only thin (few tens of nanometers thick) samples can be examined at $U_0 \leqq 50$ kV. Energy loss in the sample depends on sample composition and thicknessEgerton (2011) [10]. As a rule of thumb, sample thickness should not exceed one inelastic mean free path (IMFP) at the selected incident electron energy. For carbon IMFP $\approx$ 75 nm at U_0 =50kV and $\approx$ 50 nm at 30 kV, both estimated with 10 mrad collection angle. IMFP decreases with increasing atomic number of the sample.

As discussed in Section 3.5 sampling the target 10 nm resolution conventional TEM mode requires magnification M = 10,000x to 30,000x. In TEM mode, the convergence angle $2\times\beta$, as defined by the condenser aperture is typically $\leq$1 mrad. The illumination (probe) diameter is typically hundreds of nm to a few μm. Under these conditions, a W-hairpin filament, Section 3.2, can deliver $\approx$1 nA and 6x10$^9 e^-/s$ to the illuminated area. A camera with $(1024)^2$ pix^2 would then receive $\geq$ 5,000$e^-/(s\, pix)$ yielding an adequate image SNR in most scenarios with an image acquisition time under 1s.

At the $\approx$ 10 nm target resolution of NanoMi in TEM operation mode, the contrast forming mechanism is likely limited to *amplitude contrast* that arises due to variations in sample mass thickness (ρt) and Bragg diffraction contrast in crystalline samples Edington (1975a), Carter and Williams (2016), Kohl and Reimer (2008) that leads to removal of some of the electrons by an angle-limiting objective aperture with a semiangle θ Kohl and Reimer (2008), Egerton (2005), Malac et al. (2021). Amplitude contrast that can be

[10] Mean energy loss can be used to estimate chromatic broadening due to electron interactions with the sample

interpreted in terms of ρt, rather than Bragg diffraction in crystalline materials, produces a linear response up to a large sample thickness Hayashida and Malac (2022), a fact that is important considering the short mean free path at $U_0 \leq$50 kV used in NanoMi. *Phase contrast* is unlikely to play a role under typical TEM imaging conditions used in NanoMi.

TEM amplitude contrast resolution can be understood in the same framework of chromatic and spherical aberration broadening as for STEM above, making use of the reciptocity principle Kohl and Reimer (2008). The C_S and C_C in TEM mode are those of the lens *downstream* from the sample. In the TEM case, the convergence semiangle β in Eq. 1 must be replaced by the collection semiangle γ determined as $\gamma = \sqrt{\beta^2 + \theta^2}$, with θ being the acceptance semiangle determined by an objective aperture Kohl and Reimer (2008), Malac et al. (2021)[11]. Furthermore, the energy broadening must include components from electron energy loss within the sample Egerton (2011), Kohl and Reimer (2008). The mean energy loss can be taken as an example to estimate an order of magnitude diameter of the chromatic disc in TEM d_C^{TEM}. A numerical example with C_C = 30 mm, mean energy loss E_{mean} ≈30 eV (as would be the case for a carbon sample with thickness ≈1), inelastic mean free path, λ_{in} ≈75 nm at U_0 = 50kV and γ ≈10 mrad: the resulting chromatic disc diameter $d_C^{TEM} \approx$ 40 nm. Therefore, the resolution in TEM mode is likely to be sample-limited rather than optics-limited. To achieve 10 nm target resolution in NanoMi, the sample thickness should be much smaller than λ_{in}.

In addition to SEM and STEM probe blurring and TEM image resolution loss due to spherical and chromatic aberration, we must consider electrical stability, mechanical manufacturing and alignment accuracy. As a brief example of the effect of electrical instability, we included $\frac{\delta U_0}{U_0} \approx=$ 10 ppm in Eq. 7. The instabilities of lens bias voltages for each lens can be taken into account in a similar way, although it is only the last probe-forming lens in SEM and STEM, and first lens downstream from sample (the objective lens) that have the strongest impact Kohl and Reimer (2008), Kirkland (2020).

Furthermore, care has to be taken to maintain adequate mechanical tolerances, mechanical stability of stage and source locations to keep sample

[11]TEM is usually operated with $\beta \lll \theta$, resulting in $\gamma \approx \theta$. A convergence angle $2\times\beta \approx 1$ mrad and objective aperture angle $2\times\theta \geq 10$ mrad would be typical in the TEM imaging mode.

drift[12] and vibrations at an adequate level. Similarly, noise in beam positioning electronics in SEM and STEM has to be low. These topics are discussed in sections 4 and 5 respectively. The requirements discussed in this paper provide an estimate for a generic NanoMi column. Custom implementations of specific experiments are likely to differ in some of the requirements.

2.3. Components and Their Interfaces

The electrical systems utilized in NanoMi can all be controlled by a single PC[13] running the user interface software. Fig.4 shows the system component layout and the interfaces among them. Communication to the PC is achieved through the use of USB ports to hardware that has either been purchased or custom made. From these devices comes analog input/output control, digital signals, and a series of interfaces to communicate with a scan generator, a camera[14] for image acquisition, and for the piezoelectric movers for aperture and sample positioning. Control signals (digital[15] or analog) as well as voltage levels have been listed in the figure to ensure compatibility and interchangeability of components with future NanoMi implementations. On the right hand side of both Fig. 4a) and b) is a representation of the NanoMi column indicating how each element of the column is controlled and how signals and images are collected.

3. Electron Optics

In this section we discuss the electron optics elements: Einzel lenses, electron gun, deflectors and stigmators. We begin with a brief discussion of a geometrical particle optics tool that can assist evaluation of NanoMi column layout for various applications.

[12]NanoMi sample is not directly connected to the outside of the vacuum envelope thus reducing the impact of environmental disturbances.

[13]We utilize an Intel i5 2400 and 4 GB RAM running OpenSUSE Tumbleweed Linux

[14]We now utilize Canon M50, and have experimented with Sony α6000. But for many purposes even a webcam can suffice. The communication can achieved using existing utilities, such as http://gphoto.org/.

[15]For digital communications among components we aim at utilizing https://zeromq.org/.

3.1. Ray Path Diagram of NanoMi Electron Optics

While the smallest size of SEM and STEM probe and the resolution in TEM are determined by the lens aberrations (Section 2.2, electron gun brightness (Section 3.2), convergence and collection angles (see Section 2.2), the NanoMi column needs to be designed in such a way that small probe size, desired SEM, STEM, TEM and ED functionality and desired TEM resolution can actually be achieved. In particular, the electron source needs to be sufficiently demagnified, Einzel lenses, apertures and their diameter, sample, delfectors, stigmators and signal detectors need to be correctly placed along the electron beam path. In this section we describe geometrical optics ray path visualization developed to aid design of NanoMi column layout[16]. At present the ray-path visualization is fully implemented in Matlab^{TM} with a Python implementation in progress `https://github.com/homeniukd/NANOmi_Software`.

We utilize the ABCD matrix method to trace the geometrical rays in the microscope column Liebl (2007). Using Einzel rather than magnetic lenses simplifies the matter as electrons in an electric field follow paths that stay in the same plane. When magnetic lens alternatives are considered, the electron path is helical resulting in image rotation.

Fig. 5a) shows a diagram of ray transfer by an optical element, such as an Einzel lens or free space between lenses. The element is characterized by the electron beam parameters on the *input* and *output* planes, and the transfer ABCD matrix that describes the relation of the electron beam at the input and output planes Liebl (2007). As indicated in Fig. 5a), the electron beam is described by the angle θ_1 and distance from optical axis x_1 on the input plane, and corresponding θ_2 and x_2 on the output plane.

The relation of the input (x_1,θ_1) and output plane (x_2,θ_2) is described by a transform matrix (ABCD matrix) between at the input plane. Using the simplest, thin lens approximation Liebl (2007):

$$\begin{pmatrix} x_2 \\ \theta_2 \end{pmatrix} = \begin{pmatrix} A & B \\ C & D \end{pmatrix} \begin{pmatrix} x_1 \\ \theta_1 \end{pmatrix} \tag{8}$$

E:RayTransferMatrix

[16]The same tools can be used in real time to visualize the operating mode and parameters of NanoMi.

For example, when a ray propagates in free space over a distance (z), A, B, C and D elements of the matrix are 1, z, 0 and 1, respectively. For a transfer by a lens with a focal length (f), assuming that f is much greater than the thickness of the lens, A, B, C and D can be approximated as 1, 0, -1/f and 1, respectively. A detailed description of the method can be found in Liebl (2007). Fig. 5b) shows the ray path diagram for SEM and STEM probe formation. The code calculates the convergence semiangle β and probe diameter at the sample plane. Furthermore, the estimates of Einzel lens properties in Rempfer (1985) and our own calibration of NanoMi Einzel lenses in Section 3.3 and Fig. 2f) are used to display the corresponding lens excitation $\frac{U_L}{U_0}$ and focal length f. The lens location along the beam path $z \geq 0$, with $z = 0$ mm set at the electron emitter location, can be modified by editing the code itself. The input of a lens excitation can be changed using slider with the ray path diagram updating in real time. A NanoMi SEM column that accommodates z from 0 to 550 mm and three Einzel lenses (condenser lens C_1, C_2 and C_3 placed at $z = 257$, 349 and 517 mm respectively) with minimum focal length $f \approx 6.78$ mm can achieve $\approx$ 1000x source demagnification at a sample located at $z = 529$ mm. This implies about $d \approx$30 nm diameter size at the sample plane, as limited by source demagnification, but not by lens aberrations. Replacing the W-hairpin with a LaB_6 should result in $d \approx$10 to 20 nm.

Figs. 5c) and d) show the ray path diagrams for TEM imaging and ED modes of operation. A magnification $M \approx$49,000× (49k×) can be achieved on a fluorescent screen, located at $z \approx$973 mm, in TEM mode with an objective lens (OL) at $z \approx$552 mm, first intermediate lens (I_1) at $z \approx$706 mm and first projector lens (P_1) at $z \approx$827 mm. In diffraction mode, a camera length $L \approx$400 mm can be obtained in diffraction mode in the layout with three Einzel lenses downstream from the sample plane. At $L \approx$400 mm a polycrystal lattice with 0.1 nm periodicity would produce a ring with 97 mm diameter at $U_0 = 10$ kV, 55 mm at $U_0 = 30$ kV, and 43 mm at $U_0 = 50$ kV. Taking into account the $\approx$130 mm viewable diameter of the fluorescent screen, and the up to $\approx$100 μm effective pixel of the fluorescent screen, the $L \approx$400 mm appears to be adequate.

The main difference between TEM and ED mode is that in TEM mode the sample plane is conjugated with the fluorescent screen whereas in diffraction the back focal plane of the objective lens is conjugated with the fluorescent screen Kohl and Reimer (2008), Egerton (2005), Carter and Williams (2016). Alternative column layouts can be explored using the script described here which is downloadable from NanoMi GitHub `https://github.com/homeniukd/NANOmi_Software`.

3.2. Electron Gun and Accelerator

Four types of electron guns that fall into two categories based on the physics of electron emission are widely used in electron microscopes: *thermal sources* that use high temperature to "boil off" electrons from within a small tip, and *field emission sources* that use quantum tunneling in a strong electric field to extract electrons from a sharp tip Kohl and Reimer (2008), Crewe et al. (1968), Tonomura (1987), Akashi et al. (2018) and Crewe in Valdre and Zichich (1971).

An important parameter in a microscope design is the electron source brightness B_e[17], a quantity that describes the gun's ability to deliver a beam current J into a probe diameter d with a convergence angle $2\times\beta$. A brief estimate for NanoMi W-hairpin filament ($B_e \approx 3\times10^9$)$\mathrm{Am^{-2}srad^{-1}}$) yields $J \approx 9$ pA = $6\mathrm{x}10^7$ electrons per second (e^-/s) into a d_{50} = 10nm probe at $2\times\beta$ = 10 mrad. When collecting SEM or STEM images, each 10 nm pixel would be acquired with a typical pixel dwell time between $\approx$10μs and 1 ms. Taking 30 μs as an example, the irradiation dose is $D \approx 1700\ e^-$/pix. This is sufficient to obtain adequate signal-to-noise-ratio (SNR) in SEM and bright field (BF) STEM images[18]. To increase the counts and consequently the image SNR the probe size d or convergence angle $2\times\beta$ can be increased, thus increasing image SNR at the expense of decreased image resolution, see Fig. 3. For LaB_6 with ($B_e \approx 3\times10^{10}\mathrm{Am^{-2}srad^{-1}}$) the corresponding $D \approx$ 17,000 e^-/pix within a 30 μs pixel dwell time which is adequate for most experiments[19].

The latter provide high source brightness[20] B_e, but require an additional ion pump to maintain an ultra high vacuum in the electron gun region[21]. The

[17]Values used here were scaled from brightness at 100 kV that is reported in Kohl and Reimer (2008). Source brightness is directly proportional to U_0. For a detailed analysis a brightness scaled by ΔE is more appropriate.

[18]Acquisition of a typical 1024×1024 pixel image with 30 μs dwell time takes $\approx$ 30 s.

[19]Furthermore, using electron source with high B_e allows to shorten pixel dwell time and thus the sensitivity of NanoMi to long term (tens of seconds) drift of its components or the laboratory environment.

[20]The small source size in cold field emission gun (CFEG) could simplify the design of the SEM and STEM condenser system.

[21]Schottky electron guns, also known as field-assisted thermal sources Kohl and Reimer

former provides sufficient B_e, high beam current J and can be reliably operated in mid-10^{-8} torr vacuum that can be maintained using an adequately sized turbomolecular pump (TMP), see Section 4.6. An electron gun that can accommodate either W-hairpin or LaB_6 filament appears to be a suitable solution for NanoMi.

Although an electron gun can be built in house Valdre and Zichich (1971), Hall (1966), Septier (1967), utilizing an electron gun from a decommissioned electron microscope saves significant effort and time[22]. For the current NanoMi we utilize a filament holder and Wehnelt cylinder Kohl and Reimer (2008) from gun from a JEOL-1400 series microscope, Fig. 6a), that interchangeably accommodates W-hairpin or LaB6 filaments [23] In a commercial instrument the W-hairpin and LaB_6 are mounted with their electrical feedthrough side in direct contact with the atmosphere side of the gun assembly, thus facilitating heat dissipation. But mounting the gun assembly in such a way that it is in direct contact with the vacuum chamber wall makes separation of vacuum envelope from the electron optics difficult. We utilized COMSOL simulations and experiment to evaluate heat dissipation from an W-hairpin emitter suspended in vacuum, see Fig. 6 a) and b). Electrically, the electron gun (the cathode) is floating at $-U_0$ while the anode is grounded. Therefore the heat dissipation requires use of material that is good electrical insulator and good thermal conductor. The JEOL-1400 uses ≈2 A heating current delivered to a W-hairpin filament with resistance ≈1.4Ω, generating power of about 6W. Two mechanisms dissipate heat from the gun in the NanoMi vacuum chamber: conduction and radiation (primarily from the very hot areas of the gun). Fig. 6a) shows the temperature distribution of the gun assembly mounted on Shapal-M [24] support rods and plate. Fig. 6b) shows that the gun temperature measured near the gun emission tip settles to ≈70°C. The time evolution can be described as:

$$T(t) = a(1 - b \times e^{-ct}) \tag{9}$$

(2008) are not included here. In the context of NanoMi, Schottky sources combine the drawbacks of thermal sources, i.e. the need for heating and heat dissipation, with the drawbacks of CFEG, i.e. the need for ultra high vacuum.

[22]Commercial stand alone electron guns are also available, for example, from El-Gomati et al. (2021) and `https://www.kimballphysics.com/shop/electron-gun-systems`

[23]For development of NanoMi we use W-hairpin due to its low cost.

[24]composite of boron nitride and aluminum nitride

E:GunTemp

Here T is the measured gun temperature, t is time. The fit in Fig. 6b) gives $a \approx$70°C and $b \approx$0.6632°C.The inverse of the time constant $c \approx$0.0108 min^{-1} gives a characteristic settling time $t \approx$92 min. The 92 min settling time constant indicates that the electron gun mounted in vacuum reaches to within 5% of asymptotic steady state within ≈240 min or ≈4 hrs. This is acceptable because the W-hairpin source can be operated on continuously in the 10^{-8} torr NanoMi vacuum.

In addition to heat dissipation and electrical isolation, the possibility of x-ray emission from the region between electron gun (floating on $-U_0$) and grounded anode plate has to be considered. We implemented 0.2" mm thick shielding made of 316 stainless steel attached to the anode that prevents direct line of sight from the anode-gun region to the chamber walls and viewports[25]. The angle limiting aperture of the anode opening decreases the total current downstream from the anode, thus significantly reducing the possibility of a high flux x-ray leak. The layout of the JEOL 1400 electron gun mounted on Shapal-M support plate, and the anode with an x-ray shield is in Fig. 6c)[26].

3.3. Einzel Lenses

We chose to utilize Einzel lenses for the first implementation of NanoMi, see Table 2.1. Among the reasons that motivated this decision are:

- Ease of manufacturing. Rotationally symmetric aperture-like hardware, including Einzel lens, made from materials such as aluminium, copper or stainless steel are readily machinable and suitable for NanoMi implementation.

- Conceptual simplicity. Einzel lenses are well studied and understood Rempfer (1985), Valdre and Zichich (1971), Grivet (1972), Liebl (2007), Baranova and Yavor (1989), Hawkes and Kasper (1994), Egerton (2005),

[25]The region between gun and anode is where high x-ray flux can be generated. A significant portion of the electrons that are accelerated up to U_0 is removed by the aperture of the anode thus reducing the current and the possibility for high flux x-ray generation downstream from the anode.

[26]The anode x-ray shield also modifies the electron optics of the gun-anode region.

Septier (1967), Hall (1966), Grivet (1972) [27]. Furthermore, extensive literature and practical knowledge of electrostatic optical elements exists from the days of cathode ray tube television sets.

- Einzel lenses have very low power consumption and adequate high voltage low current power supplies are affordable.

- The low power consumption of Einzel lenses implies low heat load associated with lens operation eliminating need for a chilled water supply.

- Einzel lenses have fast response, zero hysteresis and high reproducibility allowing for an easy operation.

- Images formed by Einzel lenses are not rotated relative to object, which is not the case when using magnetic lens, see Table 2.1, making NanoMi operation easier to understand.

- Einzel lenses make it plausible to eventually utilize the NanoMi components for ion beam columns.

- Einzel lenses and electrostatic component designs with patents expired exist.

- Ultra-high vacuum compatibility is easily achieved as a result of low power consumption and low heat load and the materials used for Einzel lens construction.

- Einzel lenses can be composed from small number of parts resulting in easy assembly and internal alignment of the lens components.

The two main drawbacks of Einzel lenses are, see also Table 2.1 :

- An Einzel lens can not be an immersion lens. That is, the sample must be located *outside* the electric field of the lens. This implies that focal length and lens aberrations are likely inferior to magnetic lens because aberration coefficients C_S and C_C scale with focal length f Rempfer (1985), Kohl and Reimer (2008). When increased performance

[27] Some of the books are sufficiently old to be openly accessible at public sites such as `https://archive.org/`, an aspect that can be of some importance.

of NanoMi is sought, replacement of the Einzel lens for last probe-forming and objective lens with a magnetic immersion magnetic lens may need to be considered[28].

- Einzel lenses need a high potential U_L that is comparable to U_0 on the middle electrode. While we include this in drawbacks, suitable power supplies are affordable and accessible. Furthermore, when only a limited selection of microscope magnifications are sufficient, the U_L can be obtained using voltage dividers and a single U_0 power supply as it has been in the very early TEMs.

An Einzel lens is composed of three electrodes (see Figs. 2 and 7a), b)) and can be operated in accelerating or decelerating mode Liebl (2007), ed. (2009), Hawkes and Kasper (1994). The entrance and exit electrodes are at ground potential. The centre electrode is biased to a potential U_L. In accelerating mode of the polarity of the centre electrode is opposite to the gun potential U_0 while in decelerating mode, the central electrode polarity is same as the U_0 Liebl (2007). The focal length f and aberrations of the Einzel lens are controlled by the lens potential U_L, usually quantified as ratio of the lens and acceleration potential $\frac{U_L}{U_0}$. When using Einzel lens, the energy eU of the electrons upstream from the lens is the same as downstream of the lens. In other words, the electron energy eU_0 is not changed by the Einzel lens, although the electron energy does change while *inside* the Einzel lens Liebl (2007), Valdre and Zichich (1971).

In NanoMi, we utilize the decelerating mode of the Einzel lens, with the U_L of the same polarity as the U_0. For the NanoMi Einzel lens design, we utilize the detailed study by Rempfer Rempfer (1985). Given the availability of extensive literature, we focus on practical aspects of NanoMi lens implementation. Figs. 2a), 7a) and b), illustrate the design of NanoMi's Einzel lens. The grounded casing of the lens that also serves as the two grounded electrodes is shown in red. The central electrode biased to U_L is shown in blue. The beige parts are the PEEK insulator separating the entrance and exit electrodes from the biased central (blue) electrode. Fig. 2b) shows the lens attached to the standard mounting plate. The NanoMi Einzel lenses

[28]Use of a magnetic lens excited by a permanent magnet would require a downstream lens for focusing in TEM mode and a lens before the objective lens to be used for probe-forming in STEM and SEM.

are designed such that the centre electrode is close to one of the faces of the lens. The lens can be used equally well with the "short" side (facing up in Fig. 2a) and b)), facing either upstream or downstream the electron beam. The lens in Fig. 7a) can be oriented, for example, with the short side close to the sample allowing for shorter working distance and shorter f and lower lens aberrations than in the case of an Einzel lens that is symmetric around the mid plane electrode in Fig. 7b). The overall size of the Einzel lens assembly is governed by the desired maximum U_0 and the insulator's breakdown voltage. The dielectric strength of PEEK is 18.9 kV/mm, so a minimum thickness of 2.65 mm insulator between central and and grounded electrodes is required for a $U_0 = 50$ kV NanoMi lens.

However, a more likely mechanism of failure is through flashover, a surface breakdown of the insulator, (beige in Fig. 7a) and b), where a conducting path forms between the two electrodes along the surface of the insulator. To mitigate this, the insulating pucks are grooved; it has been shown that periodic grooves in the surface of an insulator can increase the flashover voltage in a DC field by suppressing the development of a secondary electron emission avalanche Cheng et al. (2013). The grooves also serve to increase the surface path length of the insulator, as it has been found that flashover voltage increases proportionally to length for insulators with path length below 10 mm, and proportionally to the square root of length for insulators with path length between 20-50mm Naruse et al. (2015) All edges were rounded to prevent charge concentration, see Lencova in ed. (2009). The following considerations led to our choice of electrode material: aluminum is non-magnetic and has corrosion resistant properties. To improve smoothness the lens can be polished, and if needed can be electro-plated with gold to reduce oxide buildup[29]. Alternatively, non-magnetic stainless steel can be used. As insulator (beige in Fig. 2a), PEEK was chosen for its resistance to high temperature baking in a UHV system, UHV compatibility and machinability. Additionally, insulators made of organic material have been shown to have better resistance to flashover than inorganic insulators Miller (2015). Alternatively, Macor also exhibits high temperature UHV compatibility, but it is more difficult to machine, more brittle than PEEK and is inorganic with possible implication on surface flashover.

[29] We did not observe obvious surface charging due to oxide on our NanoMi even though the lens is plain polished aluminium.

Fig. 2c) depicts the lens geometrical parameters determining their electron optical properties Rempfer (1985). Here we utilize Einzel lenses with central electrode inner diameter $D_{Einzel} = 6.35$ mm with all parameters indicated in Fig. 2c). Their electron optical properties, such as focal length f, spherical and chromatic aberration coefficients, C_S and C_C, reported in detail in Appendix A of Rempfer (1985). Fig. 2f) indicates that the NanoMi Einzel lens optical properties are in agreement with those reported in Rempfer (1985). The detailed information in Rempfer (1985) is then utilized to study the effect of C_S and C_C on NanoMi resolution, see Section 2.2 and $f(\frac{U_L}{U_0})$ for column geometrical optics layout, see Section 3.

COMSOL simulations were performed for lens parameters in Fig. 2d) and e)[30], to obtain estimates for paraxial focal length f_0 and C_S. The simulation setup involves releasing electrons parallel to the optical axis with identical initial kinetic energies, at various distances from the optical axis. As they travel through the lens, they are deflected by the center electrode, as illustrated in Figs. 2d) and e). The "focal point", z_f is determined by forming a tangent line for the ray exiting the lens and extending it back until it intersects the optical axis. We find the location of the second principal plane, z_0, by extending the tangent line for the ray exiting the lens and the tangent line of the electron's initial trajectory until they intersect each other, as illustrated in 2d). The paraxial focal length f_0 (the focal length of the electron released closest to the optical axis) is given by $f_0 = z_f - z_0$. We then calculate the axial shift of the n^{th} ray to be $\Delta f_n = f_n - f_0$. Additionally, C_S is approximated by plotting Δf_n vs α^2 and extracting the slope Egerton (2005). The simulation results are compared with the data from Rempfer (1985) in Fig. (2f). We find the simulated f_0 values to be in good agreement with Rempfer (1985) as well as with 2f). The simulated C_S values have a few noticeable deviations from experimental data, but it is mentioned that the experimental error in C_S is significantly higher than for f, and only qualitative descriptions of experimental error are provided. Some drawbacks of these simulation methods include the inability to accurately calculate f_0 and C_S for $\frac{U_L}{U_0} \leq 0.5$ due to the simulation crashes. Overall, these simulation methods provide a fast and reasonably accurate method for optimizing future Einzel lens designs for lens geometries that have not already been experimentally measured in literature.

[30] $\frac{t}{D} = 0.8$ and $\frac{s}{D} = 0.7$, that is the symmetric lens design in Fig.7b).

3.4. Deflectors and Stigmators

Deflectors and stigmators are the two elements (in addition to Einzel lenses, aperture and sample holders) needed to form SEM, STEM or TEM images, or to collect an ED pattern. In this section we discuss implementation of NanoMi electrostatic deflectors, both single and two stage, and electron beam stigmators[31].

Deflectors shift or tilt the electron beam in the $x-y$ plane perpendicular to the beam propagation direction z, both for adjusting illumination in TEM and to scan the beam when collecting SEM and STEM images. A set of four plates at (as shown in Fig. 8a)) typically produces both shift and tilt simulaneously. To produce *pure tilt* or *pure shift* of the beam, two sets of $x-y$ deflector plates is needed for a total of eight plates, as shown schematically in Fig. 8b). Corresponding hardware is shown in Fig. 7c). The ratio of the upper (upstream) and lower (downstream) plates must be correctly set to produce a pure shift or tilt [32]. Fig. 8a) shows deflection angle measurements by a single plate deflector (a total of four plates, two for x and two for y) compared with calculations at $U_0 = 5$, 10 and 15 kV.

While a single mechanical design of deflector plates (Fig. 7 c)) is used throughout NanoMi, we developed two different driving amplifiers. For beam alignment we use a voltage up to ±70V for a pair of plates. However, to allow large area panning in SEM and STEM at low magnification, up to ±400 V bias is applied to the plates. The ±400 V amplifier is identical to the one used to drive the piezo movers for stage and sample positioning. The ±70 V amplifier is significantly cheaper and sufficient for all except the plates used for scanning for SEM and STEM image acquisition, where panning is required (Figs. 13,14, and Section 5.3).

The plates are spaced on 0.2" diameter in the $x-y$ plane over a 0.4" beam path along z Section 4.3 and Figs. 7c) and d). The resulting electric field is $|E| \approx$28 V/mm when using the ±70 V circuit and ≈158 V/mm using the ±400 V/mm circuit. Consequently, the deflection angle is $\epsilon \approx 800$ mrad at $U_0 = 1$kV, 27 mrad at 30 kV and 17 mrad at $U_0 = 50$ kV, all with the ±400 V power supply. The magnitude of deflection angles is adequate to achieve a

[31]Stigmators provide a means to correct azimuthal variation in lens focal length, that is they correct astigmatism of a lens Kohl and Reimer (2008), Reimer (1998), ed. (2009), Rodenburg (2004), Hawkes and Kasper (1994), Kirkland (2020), Egerton (2005)

[32]Sometimes referred to as setting the *pivot point*.

field of view (FOV) tens to hundreds of μm^2, although the distortions are large outside the central region of the FOV.

A stigmator is a quadrupole that produces focusing with focal length that can be independently adjusted for x and y directions, see Fig. 9 and 7d) Hawkes and Kasper (1994), Hawkes (1985), Liebl (2007), Egerton (2005), ed. (2009), Baranova and Yavor (1989). To allow the azimuth of the stigmator to be adjusted arbitrarily two quadrupoles offset by $\frac{\pi}{4}$ are used, as shown in the inset of Fig. 9a) and in Fig. 7d). The polarity and electric field strength of the opposing poles can be adjusted, facilitating the magnitude and azimuthal angle of the stigmator action. A quadrupole is a strong lens, therefore a rather short distance along beam direction z and $\pm$70V bias of the quadrupole plates suffices. Fig. 9 shows a measured aspect ratio of a Quantifoil grid[33] as a function of bias of the quadrupole stigmator plates. Here a 50 V bias refers to -50V to +50V bias to the appropriate plates, i.e. 100 V potential difference between plates. An aspect ratio from 1:1.05 was obtained at $\pm$50 V bias, a value that appears sufficient for NanoMi purposes.

NanoMi stigmators and deflectors plates have each *individual* plate connected to the outside of the NanoMi vacuum envelope, i.e. each plate can be accessed independently. While this is not necessary for deflector or stigmator action alone, it could allow to explore control of higher order aberrations. For this purpose, the electronics and SW control is set up to bias each of the plates relative to the ground electrode independently. This is cost efficient, with the $\pm$70 V circuits in particular, and it also allows compensation for variations in electronics reference voltages and gain.

The mechanical design, control software and electronics are described in Sections 4 and 5.2 respectively. The electronics driving deflector scanning for SEM and STEM image acquisition are in Section 5.3. The design of both deflector and stigmator pucks is very similar, see Fig. 7c) and d). They are composed of a PEEK puck with eight poles at the same $x-y$ plane for the stigmator, and four plates at the upper $x-y$ plane followed by an additional four plates at the lower $x-y$ plane for a double deflector that allows pure shift or tilt action. Deflector and stigmator assemblies have a grounded plate at the side facing the electron beam, indicated by a red arrow in Fig. 7c)

[33] As a sample, we used a Quantifoil with square mesh 7×7 μm, bar width 2 μm, on 200 mesh Au support, Ted Pella product number 656-200-AU. The inset in Fig. 9 shows the 7×7 μm square grid.

and d), to prevent charging of the PEEK insulator due to irradiation with the electron beam.

Currently, the shape of the stigmator and deflector electrodes is a simple "on edge" plate, see Fig. 7c) and d), with the sharp edges rounded off. Alternatives such as wide plates facing the electron beam have not yet been developed.

While the action of the electron beam deflectors and stigmators depends only on the strength of the electric field, i.e. only on *difference* of the plates' potentials[34], when the presence of nearby grounded elements of the column is taken into account, a symmetric bias with the same potential of opposite polarity applied to the plates is more convenient.

3.5. Detectors

To form images, the electrons must be converted to intensity I in form of digital counts located at correct image coordinates $I(x_{im}, y_{im})$ Rez et al. (1992), Reimer (1998), Kohl and Reimer (2008). In TEM and ED mode, this is achieved by taking an image of a scintillator (SC) screen Fig 1a) and Section 3. In TEM and ED modes, all pixels of the image are collected simultaneously. In SEM and STEM mode, the image is collected pixel by pixel (in serial mode) with either the secondary electron count (SE) in SEM or transmitted electron count in STEM assigned to each position of the probe x_{im}, y_{im}. Electrons are detected through conversion of electrons to light utilizing a suitable SC Reimer (1998), Kohl and Reimer (2008). Direct detection of electrons is indeed possible, offers high detector quantum efficiency (DQE), but is not considered for NanoMi due to their high cost.

In SEM and STEM mode, electrons are detected by SC followed by a photomultiplier tube (PMT) or a photodiode (PD) to obtain electrical signal, Fig. 10c), and digital $I(x_{im}, y_{im})$. The current version of NanoMi utilizes both a PMT (for SEM, Everhart and Thornley (1960)) and PD (for STEM)[35],

[34] The same field strength is achieved for example with one plate at 100 V and the other at 200 V as one plate at -50V and the other at +50V.

[35] PDs have several advantages compared to PMT. They are smaller, cheaper, and can be installed in high vacuum environments. Their main disadvantage is electrical noise. In very low light conditions their signal-to-noise ratio is over an order of magnitude lower than PMTs. This could be mitigated by increasing pixel dwell time, but this solution would dramatically increase scan times. The pixel dwell time, TEM image acquisition time, signal to noise ratio and magnification requirements for adequate sampling of the TEM image has been addressed in Section 2.2.

see Fig. 10a) and b). In addition to a SC-PD stack, NanoMi's bright-field STEM (BFSTEM) detector has a Faraday cup (FC) to measure the beam current and calibrate the detectors, Fig. 10a) and b). For STEM, a PD was selected for its small size and low cost, as well as adequate performance. The entire assembly containing BFSTEM PD and FC is mounted on a 2.75" CF flange, Fig. 10a) and can be retracted from the electron beam when TEM images are collected on SC screen mounted on the top flange of NanoMi, see Fig. 11b). A P47 scintillator and Thor Labs FDS10X10 PD has been selected. For SEM, we utilize a re-purposed Everhart-Thornley (ET) detector Everhart and Thornley (1960), Reimer (1998) mounted on one of the side ports near sample plane, see Fig. 11 b).

ET detectors can collect SEs while excluding most backscattered electrons (BSEs) Reimer (1998) utilizing the energy and angular distribution differences between SEs and BSEs Reimer (1998). Scattering angle discrimination between SEs and BSEs is achieved by detector placement relative to the sample. An SE (ET) detector is placed to the side of the sample and slightly below the sample plane. This placement reduces BSE contribution, because BSEs are mostly scattered back towards the incident beam. SE energy discrimination is achieved by the ET detector's electrical design. SEs have lower ($\leq$50 eV) energy compared to BSEs Reimer (1998). The low-energy SEs are attracted into the ET detector by a grid or orifice held at $\approx$+300 V resulting in a weak electric field between the grid and sample. The trajectory of BSEs is not affected by this weak electric field. Once the SEs have entered the ET detector, they are accelerated towards the scintillator by a $\approx$+10 kV potential applied to the SC coated with thin ($\leq$100 nm) layer of aluminium, and confined to the inside of the ET detector. The $\approx$+10 kV bias ensures that SEs generate sufficient number of photons to be detected by the PMT Reimer (1998).

In TEM and ED mode, the point spread function (PSF) of the top-screen SC imaged by the digital camera, see Fig. 11b) and the resolving power of the digital camera (e.g. a Canon M50) determines the required magnification of the electron optics. As an example, the $\approx$10 nm target TEM resolution sampled by 10 pixels, i.e. $\approx$1 nm pixels[36]. A SC and a digital camera capable of resolving 10 μm at SC requires 10,000× electron-optical magnification

[36] $\geq$2 pixels is necessary as per Nyquist theorem, in practise the image is typically oversampled by a factor of 2 to 10.

for one-to-one sampling of the ≈1 nm pixel. Improving the resolution of the light optics and the digital camera or its pixel count is not necessarily beneficial, because the lateral dimensions of the excited volume of a typical SC is likely to be in the order of 10 μm or more Kohl and Reimer (2008). This is compounded by the presence of vacuum window between SC and digital camera[37], Fig. 11. The field of view (FOV) observed by the digital camera is determined by the size of the viewing window. The setup shown in Fig. 1 uses an 8" CF flange with 6" diameter SC screen corresponding to ≈15,000 pixels diameter assuming 10 μm resolvable SC pixel size. Taking into account the SC screen point spread function and possible errors arising from focusing the digital camera it is desirable to aim for a maximum NanoMi magnification ≈30,000× to ≈50,000×.

4. Mechanical Design and Vacuum Subsystem

In this section, we discuss various aspects of NanoMi's mechanical component design. We introduce both the 5" half-pipe design to support the electron-optical component (referred to as *column-A*), and an V-groove design alternative (referred to as *column-V*) suitable for a horizontally positioned NanoMi column Rempfer (1985), see Fig. 11. We discuss the materials used to manufacture the electron-optical components and their support, the sample and aperture holder designs.

4.1. General Column Layout

The main goals of our mechanical design were modularity, ease of alignment, manufacturing simplicity, low cost and rapid assembly and disassembly. We have two basic design layouts for the NanoMi: an arbitrary orientation column configuration (column-A) using a 5" half pipe to support the electron-optical elements, and a horizontal column configuration utilizing a V-groove for electron optical element support (column-V), see Fig. 11 and Rempfer (1985) [38]. Both column-A and column-V enable alignment of

[37]An alternative scheme for TEM and ED could involve implementing a SC with a camera placed inside NanoMi's vacuum. A chip extracted from a webcam with a thin SC may prove to be an alternative solution.

[38]As implied, the 5" half-pipe design can be used in any orientation, while the V-groove is particularly suited for horizontally mounted electron-optical test bed Rempfer (1985). Both designs use the same outer diameter lens and deflector pucks, Fig. 7 that

the electron-optical components outside the vacuum envelope (e.g. on a table top) and flexible placement of the electron-optical components along the beam path. The column-A half pipe has tapped holes every $\frac{1}{3}$", analogous to an optical breadboard[39]. For column-A and column-V systems, the high and low voltage wiring feedthroughs all pass through the base chamber to simplify the vacuum envelope and centralize the wiring. Standard CF flanges are utilized for all vacuum, light optical and electrical flanges.

Typical machining tolerances (±0.001") are sufficient for alignment and alleviate the need for mechanical adjustment screws accessible from outside the vacuum envelope. The 5" half-pipe can be removed in one piece enabling components to be positioned for a customized column layout, see Fig. 11a) and b). Components are bolted to standard mounting plates that match the inner diameter of the half pipe to keep them on the beam axis, see Fig. 7e). The 5" half pipe bolts onto a three rod frame, indicated in cross section in Fig. 7e). Electronic CAD files for the mounting plate and the half pipe are provided in Section 14. Low voltage (i.e. below 1 kV) wiring for stigmators, deflectors and piezoelectric movers, is connected to vacuum-sealed 25 pin sub-D (DB25) connectors that allow quick removal and installation.

The column-V configuration uses a V-groove and the components' fixed 2" outside diameter to keep them aligned to the beam axis, Fig. 11c) and d). The electron optical axis is 1" from the element edge. Using the column-V design, the components can be placed at arbitrary locations along the beam path, rather than at a limited number of locations determined by pre-drilled holes as in the column-A design. Tapped holes for hold down plates are bread-boarded every $\frac{1}{2}$" on the side of the V-groove, but they do not need to coincide with a location of an electron optical element. In column-V setup, a rectangular chamber with a hinged top cover allows easy access, Fig. 11c). Therefore, it is not necessary to remove the optical components including the V-groove from the vacuum chamber for adjustments[40]

are mounded on an universal mounting plates when using the column-A set up, or directly placed in the V-groove of the horizontal column-V.

[39] We chose standard dimensions rather than metric because of the availability of standard sized material and hardware in North America.

[40] Current NanoMi prototypes are mounted on an optical table with air legs for vibration damping, but this is not necessary and will depend on building conditions where the instrument is located. We expect that vibration criterion VC-D standard should be sufficient for the target specification resolution of ≈5 nm, better than NanoMi's target of

.

The insulating parts of deflectors, stigmators and Einzel lens are all made from PEEK. PEEK is mechanically stiffer than e.g. Teflon and so it is better at maintaining dimensions than Teflon. The rods that isolate the electron gun from the ground plate are made of Shapal-M, a machinable ceramic. Shapal-M has good thermal conductivity which is why we chose it for the gun mounting to conduct away the heat generated by the W-hairpin filament, Section 3.2. Both PEEK and Shapal-M are UHV compatible and allow for vacuum bakeout to ≈150°C.

4.2. Einzel Lens Mechanical Design

The reasons for selecting Einzel lens for initial NanoMi are discussed in Sections 3.3 and 2.1. The consequent need for $U_L \approx U_0$ requires design that adequately isolates HV components. In order to prevent flashover arc, corrugations are added to the insulator to increase surface length as can be seen in the lens cutaway (Fig 2). Puncture arcs are prevented by using sufficient thickness of insulator (PEEK). The metal parts of the lens is made out of aluminum for reasons mentioned in Section 2.1. Rounded edges are critical to prevent field enhancement and arcing ed. (2009). The central electrode of the Einzel lens is fully encased in a 2” diameter grounded cylinder and endcaps that serve as the entrance and exit electrodes Liebl (2007), Rempfer (1985) to prevent arcing to other column elements. The lens is made in both asymmetric Fig. 7a), and symmetric design, Fig. 7b). The asymmetric design is used to achieve, for example close distance of the lens optical centre to sample plane. The symmetric design can be of use where beam needs to enter or exit the lens at large angle without getting blocked by the lens hardware. The Einzel lens overall size is determined by the need to electrically isolate the middle electrode at $U_L \approx U_0$ from the ground entrance and exit electrodes[41].

4.3. Stigmator and Deflector Mechanical Design

The reasons for selecting parallel plate electrostatic stigmators and deflectors is discussed in Section 4.3. Beryllium copper pates are held in PEEK puck, Fig. 7c) and d). Since PEEK is an insulator and would charges when

≈10 nm.

[41]Curently, our lens operate at ≤20 kV as dictated by the need to reduce high energy x-ray generation prior to instrument completion. Testing at $U_0 = 50$ kV is pending.

irradiated by an electron beam, conductive shields are used to prevent electron beam from reaching PEEK parts, see Fig. 7c) and d). A screw mount is provided for each plate to allow convenient electrical connection of the grounding plate, the $\pm$70 V and the (in case of SEM / STEM scan plates) $\pm$400 V power.

A deflector that enables pure shift or pure tilt, Section 3.4 is composed of two sets of four plates with 0.03" width and 0.4" length along beam direction z separated by 0.2" along z, i.e. eight plates in total, Fig. 7c) and 8. The current design of NanoMi stigmator uses a single set of eight plates with 0.03" width and 0.4" along the beam direction z, Fig. 7d) and 9. The deflector and stigmator plates are separated by 0.2" in the $x - y$ plane perpendicular to the electron beam. The electronic circuitry is discussed in Section 5.3 and 5.2.

4.4. Aperture and Sample Motion

We opted for piezoelectric slip-stick motion with 10 mm travel and $\approx$20 nm step, Fig. 12. This way, only low current 1 kV power needs to be provided from outside the vacuum envelope to position apertures and sample[42].

We utilize the slip-stick motion scheme Pohl (1987), Tapson and Greene (1993). The design uses magnetic stainless steel and rare earth magnets. However, the presence of the magnets does not observably affect NanoMi's electron beam because the magnetic fields are contained within the piezo-mover actuator which is sufficiently far from the electron beam path. Since each axis only requires one small gauge wire rated to $\approx$1000 V, we are able to accommodate many movers on a single sub-D (DB25) vacuum feedthrough. Slip stick motion is well suited for this application because it only voltage pulse to achieve motion, but once it has moved, the actuator is at ground potential. Slip stick motion can also achieve long range motion in small steps, we opted for 10 mm maximum travel in 20 nm steps. The aperture and sample assemblies can be used in any orientation, making placement close to the face of asymmetric Einzel lens possible, Fig. 12d) and 1b). At present, the sample positioning system offers only motion in the $x - y$ plane and no z-height adjustment or sample tilt. At this time, NanoMi does not

[42]Traditionally, apertures and sample movement is achieved through mechanical-vacuum feedthroughs with motors placed outside vacuum. Using our set up makes it easier to build a column that is independent of its vacuum envelope. Moreover, the piezoelectric set up for NanoMi is UHV compatible.

have a vacuum load-lock, therefore sample exchange requires column venting. However, the sample holder can accommodate up to nine 3-mm diameter TEM grids, see Fig. 12 for set up with five positions, and only takes a few hours to pump down. If needed, a load lock can easily be added to one of the 6" ports at the sample plane, see Figs. 1 and 11. Information on the electronics to power the movers is in Section 5.4.

4.5. Vacuum Compatibility of Materials and Components

In addition to desired mechanical and electrical properties, the materials used for NanoMi's electron-optical components need to be non magnetic, UHV compatible and bakeable. Metal components exposed to electron beam must be made of materials that are easily polished and cleaned, and that do not form surface oxide to avoid charging. For these reasons, we use 304 or 316L stainless steel, 6061-T6 aluminum, beryllium copper and PEEK for most components. They can be baked to 150°C. Standard off-the-shelf UHV Conflat Flange (CF) components such as chambers, windows, in vacuum sub-D (DB9 and DB25) connectors, etc. are used whenever possible. The piezoelectric slip stick motors use 400-series magnetic stainless steel and rare earth magnets.

Wiring below ≈1 kV uses wires with Kapton^{TM} coating for UHV compatibility [43]. High voltage wiring is implemented with internal 50 kV isolated wires[44].

4.6. Vacuum Pumping and Envelope

Here we briefly discuss the vacuum system, including chamber, pumps and gauges suitable for NanoMi. As mentioned earlier, the electron optical components are independent from the vacuum envelope, therefore the discussion here is rather generic. An existing vacuum chamber can be also used for NanoMi.

We now discuss the pumping of the NanoMi vacuum envelope, see Fig. 1 and 11b) for an example of NanoMi column-A a 6" diameter CF tubing and Fig. 11c) is used, and d). For both column-A and column-V NanoMi the envelope is bakeable to at least 150°C and suitable for UHV operation when equipped with adequate pumps. Modern turbomolecular pumps (TMP) with

[43] see for example https://www.lesker.com/newweb/feedthroughs/wire_kapton.cfm?pgid=0.

[44] We currently use http://www.jettron.com/hvla_50kv.html

several drag stages have sufficient compression ratio to achieve UHV conditions ($\leq 10^{-9}$ torr). A modern TMP has extremely low vibration, ≈10 nm amplitude, allowing direct mounting of TMP to the NanoMi chamber. The TMP is backed by a dry scroll roughing pump. Diffusion pumps are another low cost source of vacuum but we opted for the cleanliness and relative low cost of a TMP. Cryo pumping was also considered but the vibration levels can be too high. An electron gun with a W-hairpin or LaB6 filament can be reliably operated at $\leq 5x10^{-6}$ torr. In both Fig. 11b) and c), the TMP is mounted on one of the 8" diameter CF flanges near the electron source. According to our experience a ≈300 l/s TMP is sufficient to achieve adequate vacuum in a few hours with base vacuum in the low 10^{-8} torr region, see Section 14. To adopt cold field emission electron source, vacuum can be improved by adding ion pumps and differential pumping for the electron gun region. The vacuum chambers discussed here do have provisions for adding an ion pump to the column.

For monitoring typical NanoMi column vacuum we use a convection-enhanced Pirani gauge and a naked, hot filament Bayard-Alpert ionization gauge respectively, see Section 14

5. Electronics and High Voltage

In this section, we discuss the electronics and high voltage components controlling electron beam in NanoMi. Many of the electronics components were custom built, see for example Figs. 4, 14 and 13. The custom built electronic circuitry includes control of the lens voltages U_L, electron gun filament heating and U_0, deflectors, stigmators, and electronics driving pieozelectrics of sample stages and apertures. Whenever possible, the same circuitry was used for multiple purposes. For example, the ±400 V power supply driving stage and aperture positioning is also utilized to produce zoom, pan and scan driving deflectors for SEM and STEM imaging in Fig. 15. While the same ±400 V power circuit can be used for all deflectors and stigmators, this would not be a cost effective. We have therefore developed a low-cost ±70 V version to drive all deflectors and stigmators except for the main deflector set used for SEM and STEM image acquisition.

The lenses and electron gun require high voltages on the order of tens of kilovolts and a circuit with appropriate standoff distances was designed for them. Sample stage, aperture positioning and beam scanning operate at or below ±400 V or ±70 V DC making it possible to utilize PCBs (printed circuit boards). Also, to assist in rapid integration, a commercial set of USB input/output cards were utilized to serve as the analog and digital interface between the Linux computer [45] and the custom developed hardware boards. This section will describe each circuit in detail and explain how each device is controlled from the computer and NanoMi software.

5.1. High Voltage Supplies for Einzel Lenses and Electron gun

The electron gun filament power supply output voltage is fixed at 7.5 V. Its current output is adjustable to control filament temperature. A maximum current $I_{fil} = 2$A floating at U_0 is used for the filament with typical $R \approx 1.4\,\Omega$. U_0 is provided by a commercial -50 kV adjustable power supply, see Section 14. Due to their affordability, each Einzel lens is currently powered by its own 30 kV adjustable power supply, Section 14. Lens voltages are set manually or by computer control, Section 6. A

$U_0 \leq$30 kV is currently utilized to allow for $\frac{U_L}{U_0} \approx 1$ using the existing $U_L = 30$ kV lens power supplies. The control of both U_0 and U_L is implemented by 0 to 10 V control voltages that correspond to zero to full scale of each power supply, see Fig. 4. A 50 kV power supply is costly, therefore we are developing a voltage divider to provide U_L for all lenses from a single 50 kV power supply.

5.2. Deflector and Stigmator Electronics

In this section, we discuss the power circuitry and control of the ±70 V electronics driving the deflector and stigmator plates, and the ±400 V power supply electronics driving the deflectors used for SEM and STEM zoom, pan and image acquisition. The use of ±400 V circuits that are also used for the piezoelectric sample and stage moves, Fig. 14, for SEM and STEM imaging is driven mainly by the desire to allow for a large pan range, see Fig. 15. The ±70 V option, Fig. 13, can be also used for SEM and STEM, but would allow only for reduced pan area. ±70 V is sufficient for column alignment purposes.

The amount of deflection or the strength of a stigmator depends solely on the electric field between the active plates and their distance apart. The electric field in turn depends only on the potential *difference* between the plates. Therefore it would appear that a set of (deflector or stigmator) plates can

[45] Based on Intel i5 2400 with 4 GB RAM

be driven for example by amplifiers providing only positive voltage. A 50 V potential difference can be then obtained by, for example, applying 20 V and 70 V to the individual plate. This would simplify the circuitry significantly. However, when nearby grounded electrodes are taken into account symmetric power supplies appear to be a conceptually and practically simpler solution. The 50 V difference above is then produced by -25 V and + 25V circuits referenced to the microscope ground [46]

As mentioned above, the same ($\pm$70 V or $\pm$400 V) circuitry is used for each deflector or stigmator plate. Therefore we developed a circuit, see Fig. 13, for the $\pm$70 V, and a PCB board that has four channels that can be individually populated and used individually. A single four channel board can be used to drive either one set of deflector plates or one axis of a stigmator. Each of the four channels are identical and contain a voltage buffer, an amplification stage using a digital potentiometer as a feedback resistor, a panning stage that allows shifting of the signal, and finally a stage that amplifies the signal to high voltage. The panning stage for channels two and four inverts the signal relative to channels one and three to achieve symmetric bias around ground potential. To power a stigmator or a deflector for pure shift or pure tilt, two boards are required to provide eight channels. Utilization of identical boards aims to ensure modularity and make it easier to reproduce NanoMi. Each of the channels can be individually controlled from the Linux PC and NanoMi software, in principle allowing a lookup table to be pre-programmed for pivot points at various lens settings.

For SEM and STEM image acquisition, we use an in-house built scan reference signal generator providing a $\pm$1 V reference signal, for the x and y beam position coordinates, see Section 5.3, that is used as an input for the $\pm$70 V.

The $\pm$70 V circuit is used for static deflection or beam stigmation. Four $\pm$5 V analog output values from the commercial input/output board of the Linux PC are wired to the input channels of one of the PCBs. A jumper selection allows for input of $\pm$5V (beam alignment) as opposed to $\pm$1V (scanning reference signal), see Fig. 4. To drive a single deflector, one board is required. To drive a deflector in pure tilt, pure shift (Fig. 9), or to drive a

[46] The control software includes adjustments to accommodate an offset from the ground and variation in gain among the individual circuits, making it possible to correctly "balance" each individual deflector and stigmator plate.

single stigmator, two boards are required. When used for stigmator control, all channels on the two required boards can have different voltages applied to them, and the inversion of the even channels is handled in the NanoMi control software.

5.3. Scanning Electronics

Fig. 15 shows a scan system block diagram highlighting its functionality. Fig. 15a) shows the components, starting from a PC that initiates the generation of the reference signal of desired shape, such as traditional rectangular scan or a snake pattern or any other desired scan pattern. The scan pattern is then processed by a field-programmable gate array (FPGA) that provides analog signal for the ±400 V (or alternatively the ±70 V) amplifier boards that drive the deflector plates[47]. The FPGA also digitizes the signal collected at each pixel. NanoMi software, see Section 6, allows setting of scan parameters such as the desired scan pattern, pixel dwell time, flyback time, beam parking positions etc.

The control software allows users to customize scanning parameters such as pixel count, pixel dwell time and beam flyback times, as well as allowing users to start or stop the scan by sending commands to the FPGA PCB via USB. The FPGA is programmed in VHDL, and currently generates digital x and y sawtooth scan patterns from the entered parameters [48]. The PCB for the scan unit has two 16-bit digital-to-analog converters (DACs) which convert the digital values from the FPGA into analog voltages ranging from +1V to -1V, positioning the beam in x and y. The FPGA scan unit also receives the output signal from the photomultiplier tube (PMT) or photodiode, see Section 3.5, as either a raw output current or a voltage signal from an external preamplifier circuit. For current output signals, the PCB features a transimpedance amplifier which first converts the current signal into a voltage, typically under 3.3V. The PCB features a 12-bit, 40MHz analog-to-digital converter (ADC) which samples the output signal from the PMT and sends the digitized value to the FPGA, which averages the readings for a given pixel and continuously sends the binary value, representing the

[47] The photo in Fig. 15a) illustrates the look of a complete ±400 V power amplifier, including transformers and safety enclosure.

[48] Alternative pattern shapes can be implemented. For example we are now experimenting with a "snake" scan pattern. The snake pattern was implemented in an alternative scan FPGA board programmed in Verilog.

greyscale brightness level of a pixel, via USB to the PC. The Python software on the PC receives this data and uses it to update the greyscale brightness of the pixels, forming a 2D greyscale SEM image in real-time which is displayed on the PC. The SEM image display was developed using Python's *pyqtgraph* library, which makes live line-by-line updates to the image possible.

5.4. Piezoelectric Mover Electronics

A bipolar ±400 V sawtooth output is required for each piezoelectric mover. This is achieved via use of a programmable FPGA which drives digital outputs into a 16-bit digital-to-analog converter, which then feeds two stages of amplifiers to step the voltage up to the required range, see Fig. 14[49]. A remote control is also available to jog axes, which includes the ability to change banks of outputs such that twelve outputs can be modified with a single output circuit. An UART-to-USB converter chip is also included on-board, which allows direct communication between the FPGA that drives the movers and a computer. Code has been developed in Python to control the mover over this USB link. For future work, we are developing absolute encoding to the movers to increase the repeatability and accuracy of our movements and *click-and-move* capability in NanoMi software.

6. NanoMi Visualization, Control and Modeling Software

As with the hardware (HW) and electronics, the guiding principle for NanoMi control and modeling software (SW) is to ensure modularity and ease of customization. In this section we discuss some of the already completed NanoMi SW modules. The overall layout of the NanoMi SW is in Fig. 16 and its recent graphical user interface (GUI) is in Fig. 17. The communication among SW modules and their configuration files, see Figs. 16 and 18, are such that new modules can be easily implemented either by modifying existing ones, or by developing entirely new ones. Python has been used almost exclusively and configuration files are based on XML concepts that are easily editable, Fig. 18. While NanoMi SW is released under General Public License (GPL) v3 `https://www.gnu.org/licenses/quick-guide-gplv3.html` or higher, it is possible to utilize SW modules with other license types, providing a clear interface separation exists between the GPL and non-GPL

[49]Same circuit is used to drive SEM and STEM scanning

components. The communication among components can be implemented for example using https://zeromq.org/.

6.1. NanoMi Column Layout and Visualization

Fig. 5 shows the SW module GUI visualizing a NanoMi ray path diagram in a geometrical optics approximation, see Section 3 and 3.1. The module is currently written in Matlab^{TM} although a Python version is about to be released. The slides for each of the lenses allow exploration of lens settings *off-line*, and we intend to provide a *live* Python version that would connect with NanoMi hardware in real-time in the near future. The lens ON / OFF button allows exploration of the optics with the selected lens ON or OFF, by replacing a lens with a unity matrix $I = \left(\begin{smallmatrix} 1 & 0 \\ 0 & 1 \end{smallmatrix}\right)$. The effect of electron-optical aberrations is not included in the visualization module in Fig. 5.

6.2. NanoMi Software Control

The NanoMi control software sets the status of NanoMi hardware components, such as the deflectors, stigmators, stage and aperture position as well as U_L for each lens and acceleration potential U_0. All software is written using Python and PyQt was used for the GUI from which the microscope can be controlled. The Python code was developed in a modular fashion, allowing users to integrate individual new or modified modules, see Fig. 16, into one main interface, Fig. 17, from which any of the control software interfaces can be accessed. The main program imports these subprograms that control the individual modules and creates a clickable GUI widget. This way any of the control modules can be launched at once by executing only the main Python program.

6.3. Configuration Files and Communication Protocols

As mentioned above, an important aspect of NanoMi is the ability to modify existing modules, develop new ones, and seamlessly integrate them. To that end, well defined communication among modules and their configuration files is critical. Configuration files for each module are in XML format, see Fig. 18. They hold information on each of the modules' presets for all microscope operating conditions. In Fig. 16, the configuration files in yellow (Module Preset) can hold information allowing a user to switch between modes of NanoMi operation such as TEM, SEM / STEM or ED, and their subsets (such as among magnifications in TEM or camera length in ED).

Many microscopy users have extensive experience with this mode of operation, which allows them to save their preferred settings for future use. As mentioned above, zeroMQ https://zeromq.org/ appears to provide a well defined, public definition of inter-module communication.

6.4. NanoMi Data Acquisition Software

A Canon M50 camera is used to capture and live-stream TEM images on NanoMi. The camera is mounted directly above the phosphorous screen, Figs. 11 and 1, and sends images and video capture to our Linux computer via USB. The free VLC media player software is used on the computer to display the live-stream footage. Data is then processed using ImageJ https://imagej.net/ and https://imagej.nih.gov/ij/ or GIMP https://www.gimp.org/. The live image from the Canon M50 camera is streamed and displayed using gphoto2 http://gphoto.org/ and vlc https://www.videolan.org/vlc/. The *bash* code snipplet below can be used to implement both control and live display of images, Ronchigrams or diffraction patterns on NanoMi's scintillator screen:

```
 #! /bin/sh
gphoto2 --stdout --capture-movie |
ffmpeg -i - -vcodec rawvideo -pix_fmt yuv420p
-threads 0 -f v4l2 /dev/video0 &

vlc v4l2:///dev/video0
```

The Canon M50 provides up to 24 Mpix (6000x4000 pix^2) images that may be scaled down as appropriate. We also experimented with a Sony α6000 camera with acceptable results. A suitable webcam can be also utilized. The digital camera imaging the scintillator is used to capture images, Ronchigrams and diffraction patterns from the scintillator screen. Suitable camera parameters are discussed in Section 3.5. The SEM and STEM images are acquired by digitizing signals from the Everhart-Thornley detector or photodiode, as described in Sections 3.5 and 5.3.

6.5. Lens Voltage Controller Software

Two methods of controlling the Einzel lens voltage U_L are implemented. The first is manual control using hardware voltage dividers with manual multi-turn potentiometers for coarse and fine adjustments. It was used for the initial testing of individual lenses and has been updated to computer control of the lenses using the NanoMi control SW interface, Figs. 16 and 17. In both cases, U_L is determined by a control voltage between 0V and 10V, where a 10 V control voltage corresponds to the maximum voltage provided by a power supply, e.g. 30 kV for a Spellman model X3000 or Bertan model 2554-2. Using the SW control, the 10 V control voltage for each lens U_L supply is produced by a single digital to analog converter channel. In addition to setting, loading and saving U_L for each lens for various modes of operation, the SW interface allows application of a U_L *wobble* to any of the lenses. The wobble is useful for alignment of the electron beam, see Section 7. Both the magnitude of the wobble (typically ± 10 % of U_L), and its frequency (typically 0.1 Hz to 10 Hz) can be set by a user. As with other modules, the U_L control module has been developed in Python and the user GUI was implemented using PyQt. The lens U_L control module allows easy set up of the desired number of lenses applicable for a NanoMi column.

7. NanoMi Column Assembly and Alignment

Here we discuss some of the aspects of NanoMi column assembly and alignment. The assembly aspect is rather straightforward, although vacuum cleanliness protocols should be followed to avoid excessive contamination and possibly electrostatic charging or surface breakdown of contaminated components. A NanoMi column bake to $\leq$150°C after the column has been assembled or after it was vented is a good practise that prevents contamination issues. In our experience, replacing samples or components followed by an overnight bake eliminates detectable charging issues.

The NanoMi electron optics alignment consists of two steps. First, components need to be mechanically aligned on the 5" half pipe breadboard, Figs. 1b) and 11a) and b). The accuracy of this step is determined primarily by the accuracy of machining and accurate component fit, Section 4. After the half pipe has been mounted on the studs of the lower chamber with the electron gun and anode, we use a laser pointer mounted near the far end of the 5" half pipe (almost at the plane of the fluorescent screen) to finalize the position of the 5" half pipe relative to the electron gun. A careful centered placement of a low power laser pointer on a lens mounting plate adapted for the laser pointer and placed near the distant end of the 5" half pipe is used to center the 5" half pipe relative to the Wehnelt cylinder opening of the electron gun. When misaligned the laser pointer strikes the cone of the

Wehnelt cylinder making it clearly observable. When aligned correctly, the laser beam "disappears" inside the gun making it difficult to observe. A small piece of paper placed at the tip of the Wehnelt cylinder can help to visualize the position of the laser beam, if needed. The alignment of the Einzel lenses, deflectors, and stigmators can be similarly verified by the laser pointer. According to our experience, the machining accuracy, see Section 4, and tight fit of components on the 5" half pipe is sufficient to achieve adequate reproducibility of NanoMi column assembly to obtain an electron beam on the fluorescent screen[50].

The next step is to align the electron optics for desired operating conditions, i.e. the operation mode such as SEM, STEM, TEM or ED and desired U_0. Here we discuss example alignment procedure for SEM and STEM, i.e. for the lenses C_1, C_2 and C_3 placed between the electron gun and sample with a deflector, referred to as *Def A*, installed between the anode and C_1 and a second deflector, referred to as *Def B* between C_2 and C_3. See Figs. 11a) and 5b). The simplified alignment procedure is based on concepts in Rodenburg (2004).

First, the W-hairpin filament is heated and U_0 is applied to accelerate the electrons down the column. Second, the beam is located on the fluorescent screen on the far end of the column, preferably with lens C_1, C_2 and C_3 near their intended operating voltage U_L^{C1}, U_L^{C2} and U_L^{C3}. The initial lens voltages can be obtained either using the ray path visualization of the column in Section 3, or experimentally. With the lenses near their operating conditions the following procedure appears to quickly lead to rough alignment of NanoMi SEM / STEM column with a W-hairpin filament:

1. Retract apertures and remove sample from the beam.
2. Maximize the apparent brightness of the beam on the fluorescent screen using *Def A* while keeping U_L^{C1} unchanged near its intended operating conditions. This step can be substituted and better alignment likely obtained by the "cat eye" procedure for gun alignment Kohl and Reimer (2008).
3. Adjust the U_L^{C3} to near its intended operating value, presumably with a cross over at the sample plane. Wobble the U_L^{C3} by a few % of its

[50]Care has to be taken to place aperture and sample holders such that they do not block the electron beam. It is advantageous to keep one sample and one aperture position unoccupied to allow beam passage for alignment purposes.

intended value at low frequency (no more than 1 Hz) while observing direction of swing of the brightest area of the illumination. Use *Def B* to reduce the swing of the bright region of the illumination.

4. Check and adjust the U_L^{C1} centering using the same small wobble approach as descibed for U_L^{C3} above. Repeat the steps for U_L^{C1} and U_L^{C3} to ensure minimum swing is obtained when wobbling either of the lenses.
5. The position of the condenser aperture can be adjusted for minimum swing of the image of the aperture with U_L^{C3} wobble.
6. Insert a sample in the beam. Insert a condenser aperture in the beam. If the sample is too thick to be transparent to the electron beam, live SEM acquisition can be started and beam focusing and stigmation adjusted for maximum image sharpness in all directions in the image.
7. If the sample is sufficiently thin to be electron beam transparent at the used U_0, the Ronchigram method can be used: the $U_L^{C_3}$ is varied until a cross over, i.e. infinite sample magnification patch, is observed on the fluorescent screen. The $U_L^{C_3}$ can be slightly wobbled and *Def B* alignment finalized while observing the sample Ronchigram on the fluorescent screen. With beam wobble stopped the condenser aperture is centered on the infinite magnification patch of the Ronchigram. Slight focus adjustments and stigmator corrections may be necessary.

8. Safety Considerations

Safety is the most important consideration when building an instrument. Building an electron microscope involves electrical, vacuum and x-ray emission risks. The suggestions here do not substitute for careful safety evaluation of a particular implementation of NanoMi. The most critical issues are:

- Electrical safety. The concern arises from the presence of high voltage that floats the electron gun. In NanoMi, this can be up to 50 kV. Furthermore, when electrostatic Einzel lenses, deflectors and stigmators are used, each of the elements is operated at voltages from about ±100 V to about 1 kV, sufficient to cause an injury. Example engineering controls that reduce potential problems are: reducing *total combined electrical current* of the high voltage power supplies below a limit that can cause an injury. Typically, currents below 5 mA is considered safe at any voltage xxxx (0000). Furthermore, it is important to take into account energy stored in capacitors. Furthermore, proper grounding, enclosure and interlocks as well as automated fast shut off switches in the circuitry should be implemented. Bleeder resistors should be set up to drain charge from capacitors when the power supplies are turned off. https://www.standards.doe.gov/standards-documents/1000/1092-BHdbk-2013/@@images/file

- X-ray safety. Electrons generate x-rays when accelerated or decelerated. At 50 kV electron energy, the generated x-rays can penetrate considerable thickness of many materials. Care therefore needs to be taken to use sufficient material thickness, or material with high atomic number to absorb the x-rays[51]. Alternatively the operating energy of NanoMi can be decreased to limit the energy and penetrating power of the generated x-rays. For many experiments a low energy, such as 1 keV to 30 keV could be preferable to high energy (e.g. 50 keV) electrons. The x-ray flux is related to the electron beam current that is being decelerated or accelerated. Therefore, the region between the electron source and the anode itself, where many electrons are stopped by the anode aperture, is of particular concern. Later in the column, the beam current is significantly lowered also lowering the x-ray flux. Design considerations can significantly reduce x-ray exposure risk. For example, using a stainless steel vacuum chamber instead of aluminium decreases the x-ray attenuation length by a factor of 2 to 3. Reducing electron energy from 40 keV to 10 keV decreases the attenuation length about 100 times in both materials. Therefore, high atomic number material should be selected and the lowest electron energy suitable for the application should be utilized[52]. Regardless the particular set up, it is desirable to have the NanoMi column reviewed by local x-ray safety authorities[53].

- Vacuum safety. Vacuum vessel can implode at 14 psi atmosphere. Design the vessel with sufficiently thick wall if custom designing. CF

[51] Use of leaded vacuum port windows rather than standard glass or silica windows maybe preferable.

[52] Sample thickness, desired probe diameter and the source brightness limit the smallest usable electron energy.

[53] Often universities or hospitals may have ability to review and certify x-ray equipment safety.

hardware is safe and often uses chambers with a circular cross section to better distribute forces

Additional risks can arise, for example, from presence of hot surfaces during vacuum chamber bakeout, wiring posing a tripping hazard and cryogenic and suffocation hazard from use of liquid nitrogen. Obviously, the system should be de-energized, including draining charge from capacitors, when modifications to its electrical and vacuum components are made. Furthermore, some of the components may be heavy enough to cause an injury when not handled with care. The list here is not exhaustive, additional risks may be applicable to a particular implementation of NanoMi. Furthermore, the rules and regulation that the instrument must comply with likely vary among jurisdictions.

9. Licensing Considerations

NanoMi is distributed under two different licenses: General Public License (GPL) version 3 or higher, and CERN weakly reciprocal license version 2 (CERN w.r. v.2). NanoMi software, including but not limited to NanoMi control, optics and electronics simulations are subject to GPL. All hardware and its design, including mechanical drawings, vacuum layout, electron optical elements and all electronics circuitry are covered by CERN w.r. v2. The licensing arrangement was selected to maximize access to the software aspect of NanoMi while maintaining suitability of hardware for commercial applications while not affecting pre-existing intellectual property. The guiding principle is that NanoMi hardware components and designs can be used in commercial instruments and *only changes and modifications of NanoMi component* utilized for commercial purposes has to be provided back to the NanoMi community. The non-NanoMi components of commercial instruments are not affected by the utilization of NanoMi hardware and hardware designs. NanoMi hardware component blueprint updates need to be provided back to the NanoMi project without undue delay. Although the aim is to ensure that NanoMi software is publicly available under GPL v.3 or higher, it is possible to utilize non-GPL components in NanoMi. In such a case however, a clear separation between the GPL and non-GPL component must be implemented. An example of such separation would be an stand-alone non-GPL code communicating with the GPL licensed NanoMi software over a clear and well defined interface, e.g. the above mentioned https://zeromq.org/.

10. Summary

We provide comprehensive information on an open source electron microscopy platform, called NanoMi. While the instrument is still not fully integrated to offer seamless SEM, STEM, TEM and ED capabilities, its components are tested and interfaces among them are well defined. Some of the components can be used separately from NanoMi. While NanoMi's main goal is to provide easy to build training instruments, with capabilities that are unlikely to compete with high end commercial machines, NanoMi also provides a toolbox of components suitable for development of custom experiments and integration with existing apparatuses, such as thin film growth chambers, AFM and STM instruments or optical benches. For its initial incarnation, we chose electrostatic Einzel lenses and electrostatic deflectors and stigmators. However, magnetic coil or permanent magnet excited lenses can be integrated as needed. The current electrostatic optics could make the NanoMi column amenable to use with ion beams. The components are designed for a maximum operating voltage $U_0 = 50$ kV, although the cost can be significantly reduced when $U_0 \leq 30$ kV. We provide information on safety that needs to be considered in the design and operation. The software for NanoMi instrument control and modeling is designed to provide maximum freedom and deep insight in concepts underlying electron microscopy. The modularity of the software, hardware and electronics components, together with well defined interfaces and configuration files, aims at making expansion and customization as well as inclusion of new components in NanoMi seamless. The NanoMi software is released under GPL v.3 or higher, while the hardware is released under CERN Open Hadware Weakly Reciprocal license v.2. We chose to provide the detailed information in this paper at this early stage in the hope that other researchers may find it useful and decide to participate in the project or utilize NanoMi or its components.

11. Acknowledgment

There is a long list of people and companies that provided encouragement, useful advice and feedback as well as funding. Here we list only some of them and apologies to those who may feel omitted. Significant parts of NanoMi have been developed and built by undergraduate students. Many of them are co-authors of this paper or earlier conference proceedings, but some are also listed here. The people we would like to acknowledge for their contribution and support are: Dr. Andrew Myles, Dr. Dan Wayner, Ms. Stephanie Trottier, Charles-Antoine Gauthier and Dr. Jason Pitters of National Research Council Canada. Prof Mark Freeman and Prof. Bob Wolkow at the Department of Physics, University of Alberta were early supporters of ours. Karan Kumar, Ricky Au and Adam Prus-Czarnecki who developed the initial elements of NanoMi control software during their co-op student terms at NRC-NANO and University of Alberta. Encouragment and discussions with Prof. Hiroshi Okamoto (Akita Prefecture University, Japan), Prof. Marco Beleggia (Denmark Technical University (Denmark) and Unversity of Modena (Italy)), Dr. Yukinori Nagatani (KEK, Japan), Prof. Nadi Braidy (University of Sherbrooke, Canada), Dr. Cathal Cassidy (Okinawa Institute of Science and Technology, Japan), Dr. Ken Harada (RIKEN, Japan) and Prof. Andy Stewart (University of Limerick, Ireland) are greatly appreciated. The electron microscopy team at Hitachi High Tech, both in Japan and Canada has been supporting our efforts in building and modifying electron microscopy hardware that ultimately led to the NanoMi project. Among them, we would like to particularly thank Dr. Yoshifumi Taniguchi, Dr. Toshie Yaguchi and Dr. Takashi Fujii (all Hitachi High Tech, Japan), Mr. Charles Soong, Mr. David Hoyle, Dr. Chad Ostrander and Dr. Ian Cotton (all Hitachi High Tech, Canada) for their unwavering resolve and support of our efforts. Advice, discussions and encouragement with Dr. Masahiro Kawasaki (JEOL USA and Applied Materials, USA), Dr. Shohei Motoki, Dr. Yoshihiro Okura, Dr. Isamu Ishikawa, Dr. Hirofumi Iijima and Dr. Yuji Konyuba of JEOL Ltd. (Japan) have been supportive of our various efforts in electron microscopy for nearly two decades. Mr. Brian Legge of JEOL Canada helped us with some of the practical aspects of NanoMi operation. We are also grateful for the advice and support of Dr. Heiko Muller (CEOS GmbH, Germany). The importance of initial motivating discussions with Dr. Mike Marko (Wadsworth Centre, New York, USA) is acknowledged. We also acknowledge the support of the Natural Sciences and Engineering Research Council of Canada (NSERC), RGPIN-2016-04680 and RGPIN-2021-02539. The ongoing generous support of NRC-NANO ultimately made NanoMi possible.

12. Disclaimer

Certain commercial equipment, instruments, or materials are identified in this paper in order to specify the experimental procedure adequately. Such identification is not intended to imply recommendation or endorsement by National Research Council Canada nor is it intended to imply that the materials or equipment identified are necessarily the best available for the purpose.

References

L. Reimer, Scanning Electron Microscopy Physics of Image Formation and Microanalysis, Springer-Verlag, 1998.

H. Kohl, L. Reimer, Transmission electron microscopy: physics of image formation, Springer, 2008.

C. B. Carter, D. B. Williams, Transmission Electron Microscopy, Diffraction, Imaging, and Spectrometry, Springer, 2016.

J. W. Edington, Practical Electron Microscopy in Materials Science, part 1. The Calibration and Operation of the Electron Microscope., The Macmillan Press, 1974.

J. W. Edington, Practical Electron Microscopy in Materials Science, part 2. Electron Diffraction in the Electron Microscope, The Macmillan Press, 1975a.

J. W. Edington, Practical Electron Microscopy in Materials Science, part 3. Interpretation of Transmission Electron Micrographs., The Macmillan Press, 1975b.

J. W. Edington, Practical Electron Microscopy in Materials Science, part 4. Typical Electron Microscope Investigations., The Macmillan Press, 1976.

K. Thompson-Russell, J. W. Edington, Practical Electron Microscopy in Materials Science, part 4. Electron Microscope Specimen Preparation Techniques in Materials Science., The Macmillan Press, 1977.

C. E. Hall, Introduction to electron microscopy, 2nd ed, McGraw-Hill, 1966.

P. Hawkes, U. Valdre, Biophysical Electron Microscopy, Basic Concepts and Modern Techniques, Academic press, 1990.

P. W. Hawkes, E. Kasper, Principles of electron optics. vol. 1-3., Academic Press, 1994.

P. Grivet, Electron optics, 2nd English edition, Pergamon press, 1972.

U. Valdre, A. Zichich, Electron Microscopy in Material Science, Academic Press, 1971.

H. Rose, Geometrical Charged Particle Optics, Springer, 2009.

B. M. Siegel, Modern Developments in Electron Microscopy, Academic press, 1964.

R. F. Egerton, Physical Principles of Electron Microscopy, Springer Verlag, 2005.

Open Science Foundation, Nanomi - an open source transmission electron microscope, https://osf.io/bpj73/, 0000.

NanoMi, Nanomi GitHub, https://github.com/homeniukd/NANOmi_Software, 0000.

M. Malac, M. Cloutier, M. Salomons, S. Chen, S. Yakubu, M. Leeson, J. Pitters, D. Vick, D. Price, D. Homeniuk, M. Hayashida, R. Egerton, NanoMi: An open source (scanning) transmission electron microscope, Microscopy and Microanalysis 26 (2020) 1810–1811.

M. Malac, K. Kumar, D. Wen, J. A. Marin-Calzada, M. Cloutier, M. Salomons, D. Homeniuk, S. Chen, J. Pitters, D. Vick, D. Price, M. Hayashida, R. Egerton, NanoMi open source (s)tem platform: Initial sem implementation, Microscopy and Microanalysis 27 (2021) 1062–1063.

M. Malac, D. Homeniuk, M. Kamal, J. Kim, M. Salomons, M. Hayashida, J. A. Marin-Calzada, D. Vick, D. Price, R. Egerton, NanoMi: An open source electron microscope component integration, Microscopy and Microanalysis (2022) 0000.

R. F. Egerton, Electron Energy Loss Spectroscopy in Electron Microscope, 2011.

H. Liebl, Applied Charged Particle Optics, 2007.

A. Delong, B. Lencova, Early history of electron microscopy in czechoslovakia, Chapter in Advances in Imaging and Electron Physics (2021). doi:DOI:10.1016/bs.aiep.2021.08.006.

L. A. Baranova, S. Y. Yavor, The optics of round and multipole electrostatic lenses, Advances in electronics and electron physics 76 (1989) 1–207.

J. O. ed., Handbook of Charged Particle Optics, 2^{nd} edition, CRC press, 2009.

A. Septier, Focusing of Charged Particles, Academic Press, 1967.

G. F. Rempfer, Unipotential electrostatic lenses: Paraxial properties and aberrations of focal length and focal point, Journal of Applied Physics 57 (1985) 2385.

E. J. Kirkland, Advanced Computing in Electron Microscopy 3rd edition, Springer, 2020.

R. Egerton, M. Watanabe, Spatial resolution in transmission electron microscopy, Micron 0000 (2022) 0000.

T. Ogawa, Y. Yamazawa, S. Kawai, A. Mouri, J. Katane, I.-Y. Park, Y. Takai, T. Agemura, A novel monochromator with offset cylindrical lenses and its application to a low-voltage scanning electron microscope, Microscopy and Microanalysis 0000 (2022) 1–13.

M. Hayashida, M. Malac, High-energy electron scattering in *thick* samples evaluated by bright field transmission electron microscopy, energy-filtering transmission electron microscopy and electron tomography, Microscopy and Microanalysis 0000 (2022) 0000.

M. Malac, S. Hettler, M. Hayashida, E. Kano, R. Egerton, M. Beleggia, Phase plates in the transmission electron microscope: operating principles and applications, Microscopy 70 (2021) 75–115.

A. Crewe, D. Eggenberger, J. Wall, L. Welter, Electron gun using a field emission source, The review of scientific instruments 39 (1968) 576.

A. Tonomura, Applications of electron holography, Rev. Mod. Phys. 59 (1987) 639.

T. Akashi, Y. Takahashi, K. Harada, T. Onai, Y. A. Ono, H. Shinada, Y. Murakami, Illumination semiangle of 10^{-9} rad achieved in a 1.2-mv atomic resolution holography transmission electron microscope, Microscopy 0000 (2018) 286.

M. M. El-Gomati, T. Wells, X. Zha, R. Sykes, C. J. Russo, R. Henderson, G. McMullan, 100 kev vacuum sealed field emission gun for high resolution electron microscopy, J. Vac. Sci. Technol. B 39 (2021) 062804.

G. Cheng, D. Cai, Z. Hong, L. Liu, Variation in time lags of vacuum surface flashover utilizing a periodically grooved dielectric, IEEE Transactions on Dielectrics and Electrical Insulation 20 (2013) 1942—-1950.

H. Naruse, H. Saito, M. Sakaki, O. Yamamoto, Flashover mechanisms of bridged vacuum gaps based on cathode electric field measurement, IEEE Transactions on Dielectrics and Electrical Insulation 22 (2015) 597—-603.

H. C. Miller, Flashover of insulators in vacuum: the last twenty years, IEEE Transactions on Dielectrics and Electrical Insulation 22 (2015) 3641—-3657.

J. Rodenburg, Understanding transmission electron microscope alignment:a tutorial, Microscopy and Microanalysis 18 (2004) 3.

P. W. Hawkes, The Beginnings of Electron Microscopy, Elsevier, 1985.

P. Rez, J. Weiss, W. de Ruijter, Acquisition hardware for imaging, Scanning Microscopy, SEM International FMF O'Hare (Chicago) IL Suppl 6 (1992) 81–94.

T. Everhart, R. Thornley, Wide-band detector for micro-microampere low-energy electron currents, Journal of Scientific Instruments 37 (1960) 246–248.

D. Pohl, Dynamic piezoelectric translation devices, Review of Scientific Instruments 58 (1987) 54.

J. Tapson, J. R. Greene, A simple dynamic piezoelectric x-y translation stage suitable for scanning probe microscopes, Review of Scientific Instruments 64 (1993) 2387.

xxxx, High voltage safety, current limits etc. osh publication or something similar that is on web for free, xxxx xxx (0000) 000–0001.

13. Figures

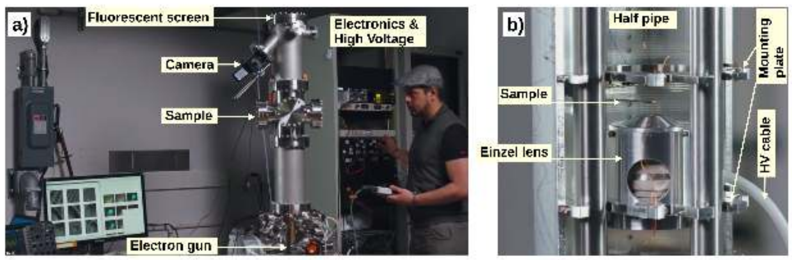

Figure 1: F:ColPhoto a) Photo of NanoMi column. This NanoMi implementation uses a vertical column with ConFlat ultra-high vacuum hardware for vacuum envelope, see column-A in Fig. 11. The column is sufficiently tall to include SEM, STEM, TEM and ED capabilities. A Canon M50 camera is viewing the fluorescent screen from a side port. Alternatively, the camera can be mounted above the fluorescent screen at the top of the column. The electron gun is located at the bottom of the NanoMi column. Locations of some of the NanoMi column components is marked. b) Photo of the inside of the column in a) near the sample area. The 5” diameter half pipe with mounting holes, a mounting plate with Einzel lens and another one for sample or aperture positioning mechanism is marked by arrows. The white high voltage (HV) cable provides U_L bias for the central electrode of the Einzel lens C_3 shown in the photo.

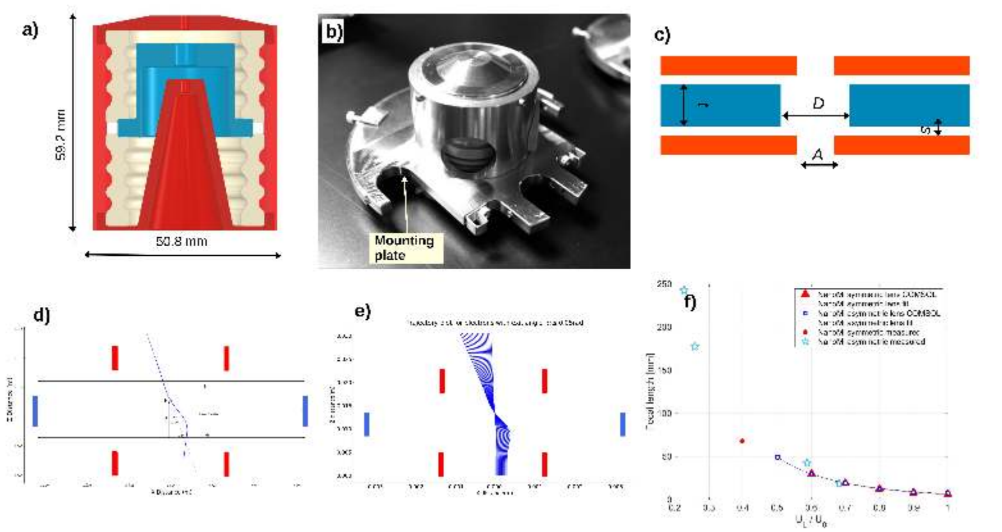

Figure 2: F:Einzel_lens Einzel lens and its optical properties. a) A cutaway view of the asymmetric Einzel lens. The central electrode (blue) is biased negatively relative to ground in decelerating mode of the lens operation. The electrically grounded cylinder and the opening in the endcaps (red) serve as the ground electrode of the Einzel lens Rempfer (1985). The beige hardware is PEEK insulator. The insulator surface corrugations for increased path length between electrodes and rounded edges to prevent field enhancement are needed for high U_0 operation ed. (2009). b) A photo of an actual Einzel lens attached to mounting base plate. c) Mechanical dimensions that determine the electron-optical parameters of the Einzel lens. Parameter convention and names identical to Rempfer (1985) were adopted. NanoMi asymmetric lens in 7 and C_2 and C_3 in Fig. 1b) has the following parameters $D = 6.35$ mm, $A = 2.54$ mm, $t = 6.35$ mm, $s = 4.445$ mm, $\frac{t}{D} = 1$, $\frac{s}{D} = 0.7$. NanoMi symmetric lens is used as C_1 in Fig. 1b) and shown in 7 b) has the following parameters: $D = 6.35$ mm, $A = 2.54$ mm, $t = 5.08$ mm, $s = 4.445$ mm, $\frac{t}{D} = 0.8$ and $\frac{s}{D} = 0.7$. d) Optical parameter definitions for an Einzel lens as used for simiulations. e) An example of ray tracing simulation for exit electron angle $\leq$50 mrad for $\frac{U_L}{U_0} = 1$. Incident electrons were released at varied distance from the lens axis parallel to the axis. In d) and e) the blue rectangles indicate an approximate location of central, negative U_L bias electrode and red rectangles indicate the location and size of ground electrodes, see a) and c).

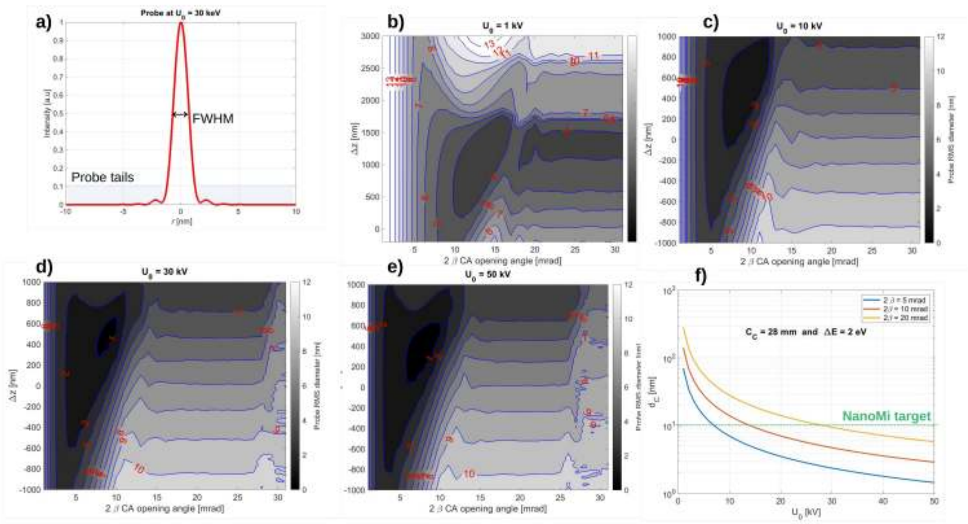

Figure 3: F:ProbeSims SEM and STEM probe diameter simulations. a) A plot probe intensity $I(r)$ dependence on the radial distance r from the probe centre $r = 0$ nm. Full width at half maximum (FWHM) is indicated in the plot. The probe tails, highlighted in grey, can contribute significant intensity to the total probe current. Probe was plotted for incident electron energy 30 keV, defocus $\Delta z = 500$ nm and convergence angle $2\beta = 5$ mrad and $C_S = 50$ mm. b) to e) Probe RMS diameter, d_{50}, that contains 50% of total beam current as a function of defocus Δz and condenser aperture size 2β at electron incident energy b) $eU_0 = 1$ keV, c) $eU_0 = 10$ keV, d) $eU_0 = 30$ keV and e) $eU_0 = 50$ keV Kirkland (2020). The spherical aberration used here was $C_S = 50$ mm, as applicable to NanoMi Einzel lens, see Fig. 2, operated at lens U_L to accelerating potential U_0 ratio $\frac{U_L}{U_0} = 0.8$, see Appendix A in Rempfer (1985). Note that the plotted range of ΔZ in b) is different from c) to e). f) Shows the effect of chromatic aberration $C_C = 28$ mm, as applicable to the NanoMi Einzel lens Rempfer (1985) at $\frac{U_L}{U_0} = 0.8$ for convergence angle $2\beta = 5$, 10 and 20 mrad. Additionally, instability of $\delta U_0 = 10$ ppm was included. The energy spread of the W-hairpin filament was assumed to be $\Delta E = 2$eV, see Kohl and Reimer (2008). Comparing the plots in b) to e) and the effect of C_C in f) suggests that convergence angle $2\beta \approx 5$ to 15 mrad. Decrease in convergence angle results in smaller effect of C_C and increase in depth of focus, as indicated by small d_{50} over a large range of Δz. But a decrease in 2β also decreases the total beam current due to limited brightness of the W-hairpin filament. Below about $2\beta = 5$ mrad, the d_{50} quickly increases due to diffraction effects at the condenser aperture. A positive value of Δz indicates underfocus, i.e. a lens weaker, i.e. $\frac{U_L}{U_0}$ lower, than in-focus excitation. A change in incident energy results in change of convergence angle when geometry of the optics (aperture diameter and its distance from cross the over) are unchanged according to $\theta = 2\lambda q$, the electron wavelength λ depends on its energy eU_0

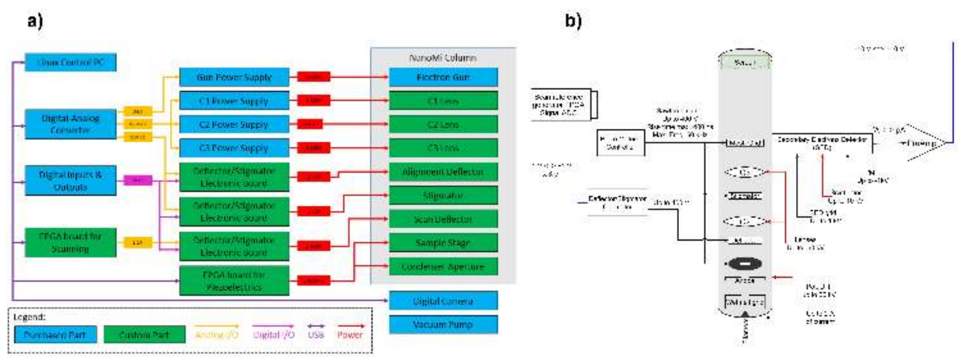

Figure 4: F:LayoutInterfaces_DH a) Layout of communication, controls and their interfaces. Solid purple lines indicate digital USB-based communication. Yellow lines are analog control, bright purple lines are digital control. All voltages are reported here to ensure compatibility of components designed in the future. Solid red lines indicate high voltage connections with voltage reported. b) Electrical connections of the NanoMi column. Lens and electron gun are at high voltage up to U_0 not exceeding 50 kV. W-hairpin or LaB_6 filament that is floating at the U_0 potential is heated with a 2 A current. Secondary electron detector, BFSTEM detector and Faraday cup signals are amplified and processed to a digital signal using ADCs of the FPGA after signal amplification. An SEM reference signal generator based on a FPGA provides reference signal controlling the beam position. TEM images or diffraction patterns are collected using a digital camera (Canon M50 in our lab) pointed at the fluorescent screen and connected directly to the Linux PC. See Fig. 16.

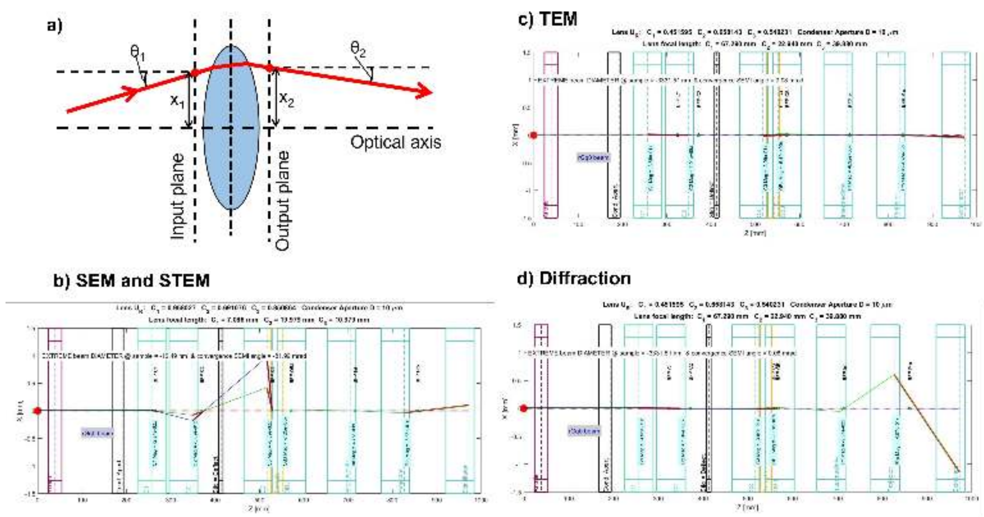

Figure 5: F:ElOpt Optics layout for SEM, TEM, STEM and ED in NanoMi. a) Parameters definitions for ABCD matrix method in geometrical optics that is used to generate ray path diagrams in b), c) and d). b) Probe forming ray path diagram for SEM and STEM. A W-hairpin filament with ≈30 μm diameter has to be demagnified ≈1,000× for 30 nm nominal probe size and ≈3,000× for nominal 10 nm probe size. Only condenser system between the electron gun (on the right and side) sample (middle of the panel) is used to form a small probe at the sample plane. c) Optics of lens downstream from sample for TEM imaging. The effective pixel size of the scintillator is a few tens to hundred μm. Therefore, to detect a 10 nm object at the sample plane a nominal magnification needs to be 20,000× or more. d) ED ray path diagram. The back focal plane of the objective lens has to be imaged onto the flourescent screen and sufficiently magnified to detect sample periodicity of 10 nm^{-1} or higher as needed for identification of structure of materials samples.

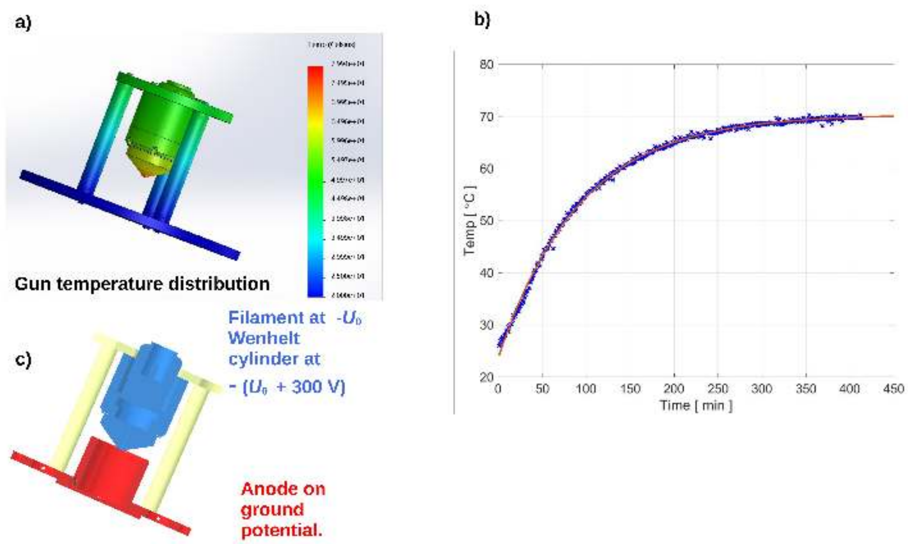

Figure 6: F:Egun Electron gun thermal stability. a) COMSOL simulations of temperature distribution on an internally mounted JEOL 1400 gun with a W-hairpin filament. The gun is supported on Shapal M rods and Shapal M mouting plate that provide electrical insulation, as needed to apply U_0 relative to ground. In JEOL microscopes, the gun is mounted with direct thermal connection to atmosphere on its high voltage connection side. In NanoMi, the gun is entirely inside the vacuum chamber with the heat conducted away by the mounting rods and dissipated by radiation as its temperature increases. Heating current $\approx$2 A and filament electrical resistance 1.4 Ω results in a need to dissipate 5.6 Watts. b) The measured temperature profile and fit. c) Shows the JEOL 1400 gun and anode assembly mounted on a Shapal M plate. The gun (marked in blue) is floating at $-U_0$ while the anode (marked in red) is on the ground potential providing electron acceleration to U_0. The x-ray shield part of the anode extends to a level close to the opening of the gun, thus reducing the possibility of an x-ray leak. The Shapal-M rod diameter is 0.5" and Shapal-M base thickness is 0.25". The diameter of anode aperture bore allowing the electron beam down the column is 1/16". The diameter of the stainless steel (316 SS) x-ray shield is 1.9" and its thickness is 0.2".

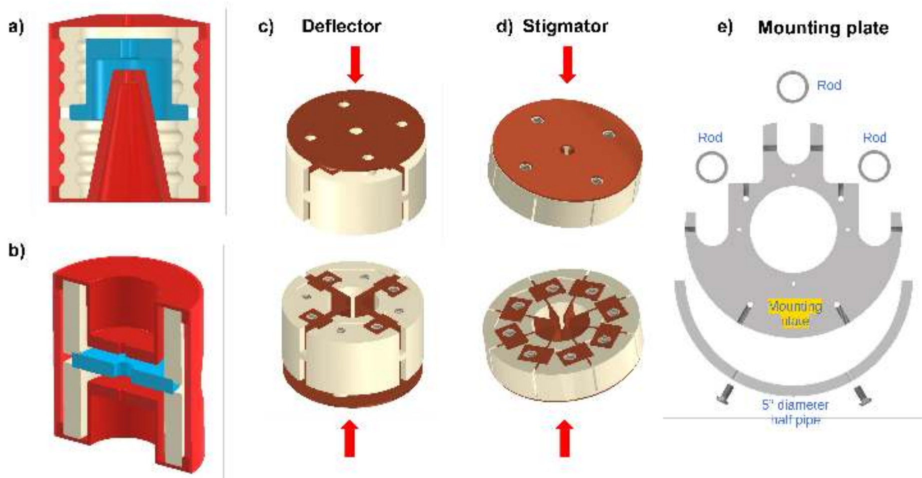

Figure 7: F:1_Mech_OptElem Mechanical layout of electron optical elements for an electrostatic NanoMi. a) Cross section of an asymmetric Einzel lens. For electron optical parameters see Fig. 2. b) Symmetric Einzel lens. The lens can be operated in both accelerating and decelerating mode. In decelerating mode, as used here, the central electrode uses the same (negative) polarity potential as the electron gun, and is drawn in blue. The grounded parts of the Einzel lens are in red and the insulator is in beige. Asymmetric lens can be oriented either in the orientation shown, or flipped vertically relative to the electron beam direction. c) Double deflector. Copper plates used as active deflecting elements are in brown. A copper ground plate is used on the surface facing the electron beam to prevent charging. Double set of plates (upper and lower) is used to provide pure shift and pure tilt capability, see Fig. 8. PEEK insulator is shown in beige. d) Stigmator comprises of 8 plates for X and Y stigmator capability. c) and d) are shown in two views with red arrow indicating the direction of the electron beam. e) Mounting base plate for the electron-optical and mechanical elements of NanoMi. The opening in the mounting plate is 2.004" to allow for mounting 2" diameter electron-optical components. The three support rods indicated in e) are 0.75" diameter. The 5" half pipe, mounting plate for the 5" half pipe and the v-groove CAD drawings included with this paper in STEP format to ensure compatibility of future components, see NanoMi5IDMountingPipe.stp, NanoMi-StandardMountingPlate.stp and v-groove.stp. For STP file format see for example ISO 10303-21 `https://www.iso.org/standard/63141.html`

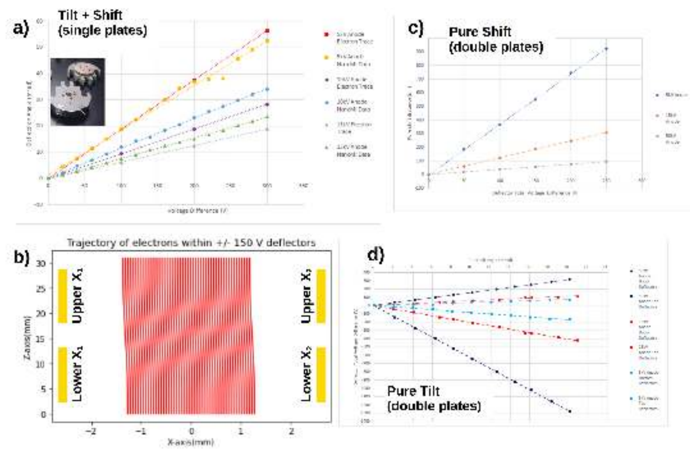

Figure 8: F:def Deflector design and electron-optical parameters. a) Deflection angle in mrad as a function of applied voltage difference between the deflector plates of a *single stage* deflector. Inset is a photo of a deflector hardware on mounting plate. Beige PEEK insulator frame and copper deflector plates as well as the copper shield facing the electron beam can be seen. The single plate deflector produces simultaneous beam tilt and shift. Measured deflection angles (labelled *data*), ray tracing (labelled *trace*) and their fit is shown for $U_0 =$ 5, 10 and 15 kV. The deflection angle decreases with increasing U_0 at a fixed deflector bias. The measured data indicates somewhat lower deflection angle than predicted by simulations. b) Conceptual simulation of electron trajectories in double plate deflector acting on parallel beam, that can produce pure shift or pure tilt. The location of a set of four plates for one direction, e.g. x is indicated in yellow. c) and d) are a calculated pure shift and pure tilt performance of the example double deflector set up in b) that uses a total of four deflector plates for each x and y direction. Since each of the plates is driven by own high voltage amplifier the ratio of the upper and lower plates can be adjusted to obtain desired pure tilt or pure shift behaviour. See Fig. 13 and 7 for high voltage amplifier and mechanical layout respectively.

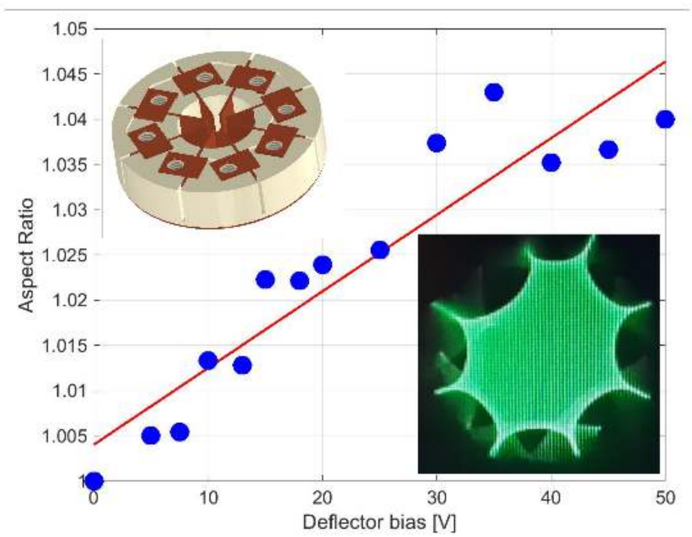

Figure 9: F:stig Stigmator is composed of two quadrupoles that are oriented 45° relative one to another in the $x-y$ plane, a total of eight electrodes. The plot shows a change of aspect ratio of squares of a Quantifoil TEM grid illuminated by a parallel beam as a function of bias of one quadrupole. A linear fit to the data $(1.00406 + 8.47335 \times 10^{-4} * V)$ is also shown (black dashed line) at $U_0 = 15$ keV incident electron energy. While the poles of the stigmator are usually paired up, we connect each individual plate element to its own high voltage amplifier (see Fig. 13) allowing for future adjustment of higher order aberrations. Furthermore, a stigmator can be also used as a simplified deflector by utilizing only four poles in total, or as a quadrupole lens to image sample or to manipulate the electron beam. Mechanical aspect of the stigmator assembly is found in Fig. 7. Upper inset shows a visualization of the stigmator assembly viewed from the side downstream of the incident beam. Bottom inset shows an example of the illuminated Quantifoil TEM grid at zero bias of the stigmator. The stigmator plates are visible as a shadow with eight-fold symmetry at the edge of the field of view.

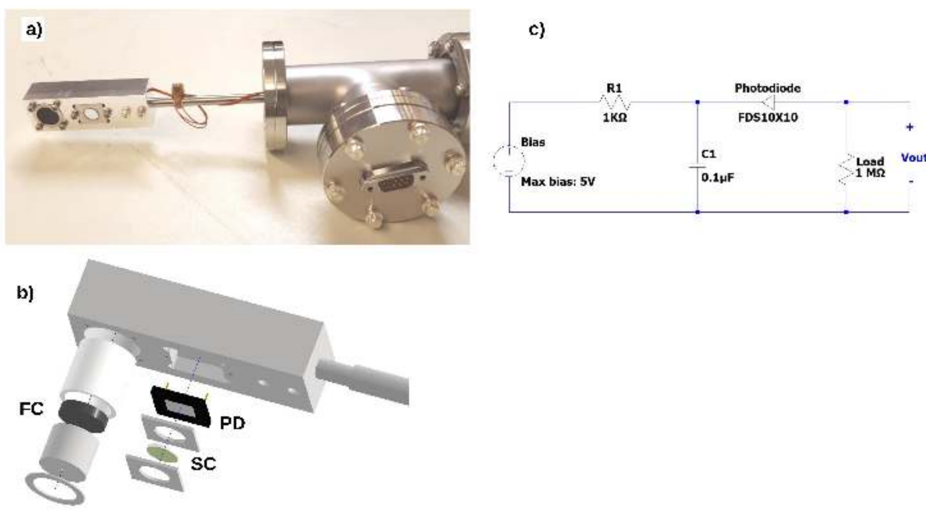

Figure 10: F:BF_Det Bright Field STEM detector implementation. a) The detector assembly consists of the detector head, incorporating a Faraday Cup (FC) and scintillator(SC)/photodiode(PD) combination; a linear feedthrough with 6" travel that permits the detector to be withdrawn from the path of the probe. A Tee flange with D-sub 9 pin connector UHV feedthrough to allow biasing of the PD and collection of the signals. b) A schematic mechanical assembly of the detector head. The FC is electrically isolated from the outer housing. A thin coat of phosphor, in our case ZnS, is applied to the face of the FC to facilitate positioning of the probe into the FC aperture by directly observing the location of the electron beam using a camera mounted on the side port, see Fig. 1a).

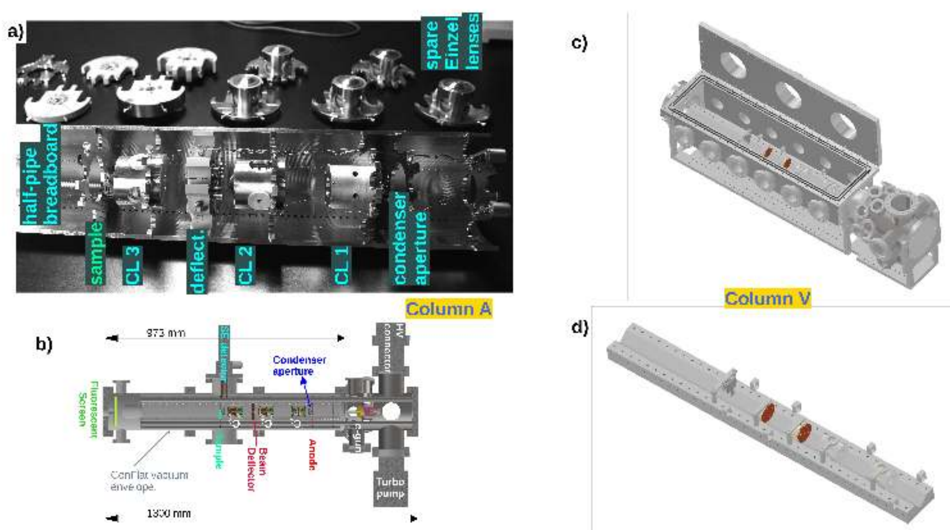

Figure 11: F:ColMech NanoMi column mechanical layout. a) Internal 5” diameter half-pipe breadboard for mounting of electron optical components, apertures and sample movers. Components are mounted and mechanically pre-aligned on the half pipe. Einzel lens, deflectors and stigmators are shown on the workbench. b) Vacuum chamber based on ConFlat hardware. In Fig. 1 the column is oriented vertically with electorn gun located at the bottom, but any orientation is acceptable. The half-pipe breadboard can be mounted in any suitable vacuum chamber. The set up in a) and b) is referred to as *column-A*. c) and d) show an alternative set up with a rectangular chamber with a hinged lid and a V-groove support for electron optical elements Rempfer (1985), referred to as *column-V*. The electron optical, and aperture and sample positioning elements are identical with a) and b). IN v-column the elements placed directly in the V-groove without the need for mounting plates. The outer diameter of all elements is kept fixed at 2”, see for example Fig. 2.

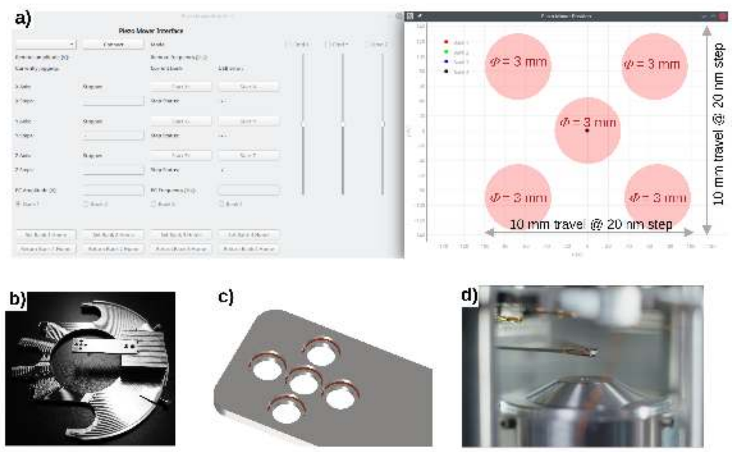

Figure 12: F:StageApt Software control and implementation of sample stage and apertures positioning piezoelectric movers. a) Software control module GUI. The example shows 3 modules (banks) controlling piezoelectric positioning system. One for sample stage and two for apertures. Three axis x, y, z, are shown although current stage mechanical design accommodates only $x - y$ in plane movement with 20 nm step over 10 mm travel range. GUI showing the location of each bank (i.e. sample and apertures) in different colors. b) Sample or aperture piezoelectric mover assembly mounted on the mounting plate that attaches to the 5" diameter half pipe using the sample mount in Fig. 7e). c) Detail of sample holder plate that accommodates up to five 3 mm diameter aperture discs or samples. d) Photo of sample holder for a single 3 mm diameter grid located near an asymmetric C_3 Einzel lens. Why do we have three banks but four banks indicated on GUI ... four color dots ?

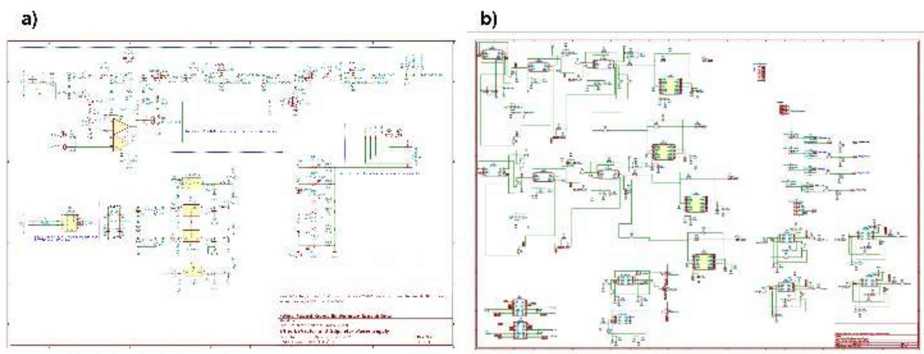

Figure 13: F:CircuitStigDef a) Circuit diagram for the power supply for the FPGA scan unit and the ±70V deflector boards. b) Circuit diagram for the ±70 V supply driving deflectors and stigmators of NanoMi. This circuit is intended to drive plates of beam deflectors and stimgators. When large area panning is required, Fig. 15, the ±400 V supply in Fig. 14 should be used instead.

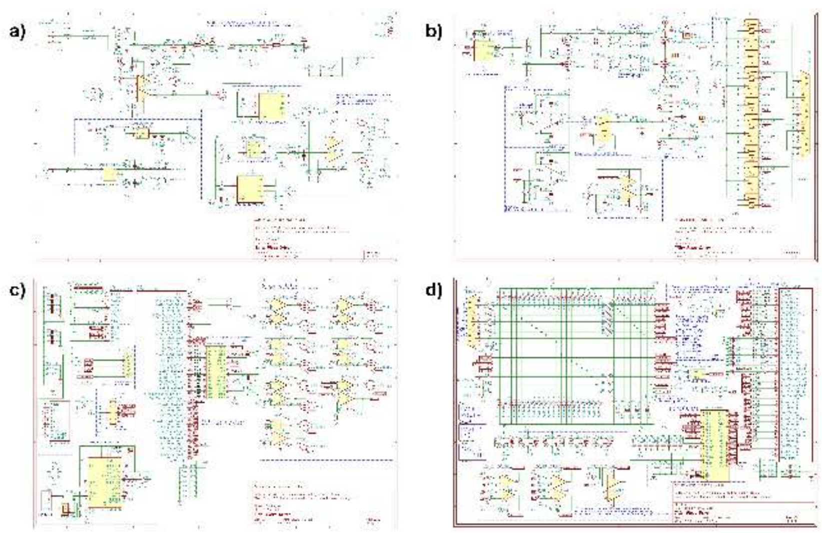

Figure 14: F:CircuitPiezoStage Circuit diagram for piezoelectric stage control. The same controller is used to position sample stage and apertures, see Fig. 12 and can be also used to drive deflector plates for beam scanning. The individual circuit diagrams are: a) Power Supply design, including a in-house developed tracking ±400 VDC amplifier, and voltage regulators providing ±12 VDC, +5 VDC, +3.3 VDC, +1.8 VDC and +1.0 VDC, all of which are used by the FPGA and other electronics in this circuit. b) Output stage design, which accepts an analog driving signal differential pair from the FPGA and/or an external single-ended ±10 V analog signal, amplifies the chosen signal up to the range of ±400 V, and outputs to a selected piezoelectric mover via relay control. The top half of the drawings are driven by two FPGA digital outputs and will force the piezoelectric output to either +400V or -400V in a matter of nanoseconds, which is required for proper piezoelectric element movement. c) FPGA outputs, where the 16-bit digital-analog converter is implemented to provide differential signals to the output stage, and where relay signals and fan control are implemented with high current abilities. The left side of the page also details the UART-USB communications and the FPGA power supplies and static voltage requirements. d) FPGA inputs, where the remote control, temperature feedback, and analog-digital converter all feed into FPGA inputs. The circuit also includes LED status indication lights for the user's benefit.

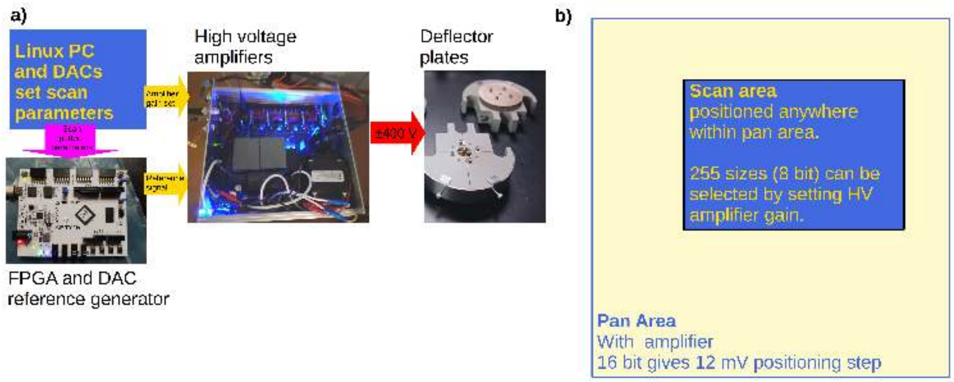

Figure 15: F:ScanSyst Layout of NanoMi scan generation system. a) A NanoMi software module sets parameters of an FPGA reference signal generator over a digital (USB) connection (magenta arrow). The FPGA generated reference signal (yellow arrow), such as sawtooth patterns for X and Y coordinates, is amplified by the high voltage amplifiers. The parameters of the high voltage amplifiers is set by the control software over a digital to analog converter. For example an x, y offset (panning) and magnification (gain) of the amplifiers are both set from the NanoMi software. High voltage, low current driving signal is then applied to the deflector plates (red arrow). A prototype FPGA board is shown here. b) Schematics indicating the zooming and panning capabilities of NanoMi scan generator. The gain, i.e. the magnification of the amplifiers can be applied in 8 bit resolution allowing 255 different values of magnification to be programmed. Using the amplifiers in Fig. 13 and 255 level resolution from 2 V to 140 V, that is $\pm$70V voltage difference, about 0.5 V step in scan amplitude, i.e. in scan magnification, is achieved. The scanned area (blue) can be moved within the pan area (yellow) over the entire field of view (e.g. 200 μm) with 16 bit resolution. The same set up is used for SEM and STEM scanning and for beam shift and tilt in TEM as well as for beam alignment, except DC voltage offset rather than scan reference signal is fed to the amplifiers. Either $\pm$ 400 V (Fig. 14) or $\pm$ 70 V (Fig. 13) high voltage amplifiers can be interchangeably used for scanning image acquisition. The panning area is determined by the maximum voltage of the amplifiers and the imaged (scan) are can be of any shape positioned anywhere within the panning area boundaries. Arbitrary scan patterns, pixel dwell times, sizes and shapes can be implemented by sending appropriate parameters from the NanoMi software to the FPGA. The signal is read back to the NanoMi software from the selected detectors, see Figs. 10 and 4.

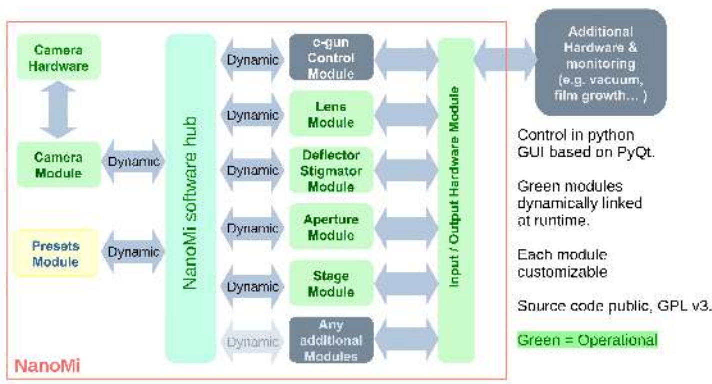

Figure 16: F:SW_layout Layout of NanoMi control and data acquisition software. Components highlighted in green are completed. A Python based modular set up has been developed allowing to select, modify and add new modules as needed. All software is run on a single (OpenSUSe) Linux PC. The *Presents module* highlighted in yellow, provides option to store user defined settings, such as a selection of NanoMi magnifications and alignments, for convenience and for novice users.

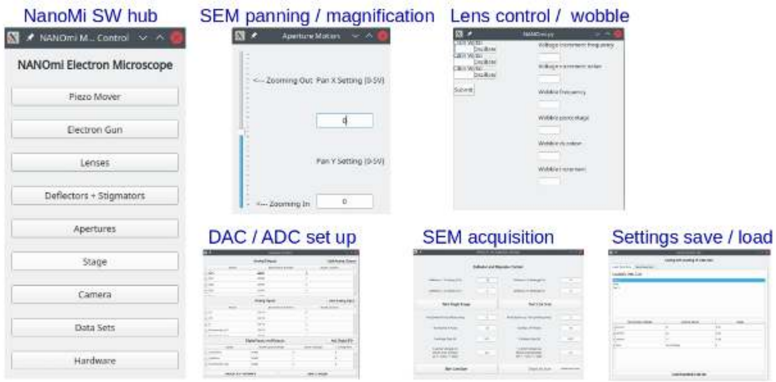

Figure 17: F:SW_GUI NanoMi software graphical user interface (GUI) has been developed using PyQt. The example GUI windows correspond to modules in Fig. 16. The main module on the left is used to open the additional windows for task or hardware specific modules. The GUI for aperture and sample position control is in Fig. 12a).

```xml
<?xml version="1.0" encoding="utf-8"?>
<dataSets>
    <!-- This is a complete data set -->
    <set name="Set 1">
        <!-- These are the individual settings -->
        <!-- "module" is the code module name they exist in -->
        <!-- "name" is the name of the variable in that module -->
        <!-- "value" is the value that was read out at the time of saving -->
        <setting module="DeflectorsStigmators" name="Def1_X" value="-4.2"/>
        <setting module="DeflectorsStigmators" name="Def1_Y" value="-1.73"/>
        <setting module="Lenses" name="C1" value="1.24"/>
        <setting module="Lenses" name="C2" value="2.48"/>
        <setting module="Lenses" name="I1" value="3.96"/>
    </set>
    <set name="Set 2">
        <setting module="Lenses" name="C1" value="0.01"/>
        <setting module="Lenses" name="C2" value="0.02"/>
        <setting module="Lenses" name="I1" value="0.04"/>
        <setting module="DeflectorsStigmators" name="Def1_X" value="2.02"/>
        <setting module="DeflectorsStigmators" name="Def1_Y1 value="3.5"/>
    </set>
    <set name="Set 3">
        <setting module="DeflectorsStigmators" name="Def1_X" value="-1.2"/>
        <setting module="DeflectorsStigmators" name="Def1_Y" value="3.1"/>
        <setting module="Lenses" name="C1" value="0"/>
        <setting module="Lenses" name="C2" value="0"/>
        <setting module="Lenses" name="I1" value="0"/>
    </set>
</dataSets>
```

Figure 18: F:1_ConfigFile An example of NanoMi software configuration file. The convention uses XML. Each element of NanoMi that is software controlled is defined here including its name, parameters and preset values. Additional modules can be added as needed Open Science Foundation (0000). See also included NanoMiDataSets.xml

14. Supplemental information

Suggestions on possible electronic files to include as supplementary information:

1. Example NanoMi software configuration file NanoMiDataSets.xml.
2. CAD drawing of 5” diameter half-pipe in STP format NanoMi5IDMountingPipe.stp for A-column set up.
3. CAD drawing of mounting plate for optical elements NanoMiStandard-MountingPlate.stp for A-column set up.
4. CAD drawing of V-groove for optical element mounting for V-column set up v-groove.stp
5. A high level parts list for minimalistic NanoMi SEM configuration.
    - Vacuum chamber, examples shown in Fig. 11. An existing chamber to suspend the electron optics column can be used.
    - v-groove or 5” half pipe to support the electron optics Fig. 11.
    - Einzel lens (Fig. 2 and 7 a) or b)) and mounting plates (Fig. 7e). For an SEM 2 to 3 lens are needed.
    - At least one deflector for beam scanning with power supply. For alignment it is desirable to use an additional deflector with a power supply placed before first condenser lens C_1. For the alignment deflector before C_1 the ± 70 V power supplies (Fig. 13) are likely sufficient, for image acquisition and panning a ± 400 V power supply is recommended.
    - A stigmator with power supply for probe forming system. The ± 70 V power supplies are likely sufficient.
    - A U_0 high voltage power supply for electron gun. (e.g. 2 to 4 A DC floating at U_0 for W-hairpin or LaB_6. Presumably an adequately sized battery can be used to supply the heating current floating at U_0.
    - High voltage power supplies for Einzel lens. Examples of high voltage power $U_0 = 30$ kV NanoMi are Spellman model X3000 or Bertan model 2554-2. A used supply can be sourced for example from ebay at a couple hundred dollars a piece.
    - A sample stage and at least one aperture mechanism with driving electronics, see Fig. 12 and 14. Since the piezoelectric movers do

not require to be energized when stationary, it is possible to share a single power supply among several stages or aperture positioning assemblies.

- Vacuum pumps. For NanoMi in Fig. 1 an Agilent TwissTor 304 FS and an IDP-15 scroll pump are being used achieving a base pressure in mid to low 10^{-8} torr.
- Detectors such as digital camera, fluorescent screen and SEM / STEM detectors (if SEM functionality is desired), photodiode with scintillator, PMT, amplifier electronics.
- Connectors and vacuum feedthroughs, D-sub 25 pin (DB25) vacuum compatible are suitable for low current low voltage ($\leq$1 kV) connections needed for deflectors, stigmators and sample and aperture piezoelectric positioning.
- An electron source. A commercial electron gun assembly from decomissioned instrument can be used. Our instrument uses W-hairpin or LaB_6 gun assembly from a JEOL 1400.
- A control PC with (USB) ADC and DAC cards. We use a tower PC based on Intel i5 2400 with 4 GB RAM.
- NanoMi control software from GitHub https://github.com/homeniukd/NANOmi_Software.
- Coated wires for internal wiring of deflectors, stigmators and piezoelectric positioning of apertures and sample. For example Polyimide coated 16 gauge wire from https://mwswire.com/.
- High voltage cables, connectors and feedthroughs for electron gun and Einzel lens.

6. Mechanical layout of electron optical elements for NanoMi column that utilizes electrostatic components[54]. All components are 2" or 50 mm in diameter. Symmetric lens is 2.2" thick, asymmetric lens is 2.33" thick, deflector is 1.13" thick, and a stigmator is 0.48" thick.
7. NanoMi control, modeling and visualization software: https://github.com/homeniukd/NANOmi_Software.

[54] permanent magnet lens were also designed, but not manufactured and tested at this time.

8. Open Science Foundation page of NanoMi project: https://osf.io/bpj73/.
9. NanoMi web page linking the various resources and column 3D visualization: https://www.nanomi.org/.
10. For inter-component communication Zeromq appears to be be suitable: https://zeromq.org/.
11. An example shell script for live stream using Canon M50 camera Start-CanonM50.sh